Geophysical Research Letters

RESEARCH LETTER
10.1029/2025GL115237

A Nutrient Effect on the TEX_{86} Paleotemperature Proxy

Ronnakrit Rattanasriampaipong[1,2], Jessica E. Tierney[2], Jordan T. Abell[2,3], and Lauren D. Gilmore[2,4]

[1]University Corporation for Atmospheric Research, Boulder, CO, USA, [2]Department of Geosciences, The University of Arizona, Tucson, AZ, USA, [3]Department of Earth and Environmental Sciences, Lehigh University, Bethlehem, PA, USA, [4]Department of Geosciences, Princeton University, Princeton, NJ, USA

Key Points:

- Nutrient stress alters GDGT distributions in marine sediments, resulting in elevated TEX_{86} values beyond those related to thermal effects
- Paleoclimate case studies from the Arabian Sea and Tasman Sea reveal that nutrient levels likely influenced the TEX_{86} proxy in the past
- Explicitly accounting for nutrient effects in the proxy system will improve the accuracy of TEX_{86}-based temperature estimates

Supporting Information:

Supporting Information may be found in the online version of this article.

Correspondence to:

R. Rattanasriampaipong, ronnakritr@arizona.edu; rrattan@ucar.edu

Citation:

Rattanasriampaipong, R., Tierney, J. E., Abell, J. T., & Gilmore, L. D. (2025). A nutrient effect on the TEX_{86} paleotemperature proxy. *Geophysical Research Letters*, *52*, e2025GL115237. https://doi.org/10.1029/2025GL115237

Received 17 MAR 2025
Accepted 6 JUN 2025

Author Contributions:

Conceptualization: Ronnakrit Rattanasriampaipong, Jessica E. Tierney, Jordan T. Abell
Data curation: Ronnakrit Rattanasriampaipong, Jessica E. Tierney
Formal analysis: Ronnakrit Rattanasriampaipong, Jordan T. Abell
Funding acquisition: Ronnakrit Rattanasriampaipong, Jessica E. Tierney, Jordan T. Abell
Investigation: Ronnakrit Rattanasriampaipong, Jessica E. Tierney, Jordan T. Abell, Lauren D. Gilmore

Abstract The TEX_{86} paleotemperature proxy is widely used to reconstruct ocean surface temperatures over the past 100 million years. However, archaeal culture experiments show that nutrient stress elevates TEX_{86} values by increasing glycerol dialkyl glycerol tetraether (GDGT) cyclization. Here, we demonstrate that this "nutrient effect" is also recorded in sedimentary GDGTs. Using an expanded core-top database, we find a significant negative correlation between TEX_{86} and nitrate concentrations ($\rho = -0.31$; $P < 0.001$) once the thermal effect is removed. There are stronger correlations (ρ −0.73 to −0.91; $P < 0.001$) in regions with steep nitrate gradients. Comparisons between TEX_{86} and $U^{K'}_{37}$-based reconstructions from the Arabian Sea and Tasman Sea suggest that nutrient stress influenced GDGT distributions during glacial-interglacial cycles. Our findings underscore the need to account for nutrient effects when applying TEX_{86} paleothermometry.

Plain Language Summary Marine archaea help regulate the global nitrogen cycle, and their membrane lipids serve as a temperature proxy (TEX_{86}) both today and in the past. While temperature is the main driver of lipid changes, lab studies show that nutrient stress also increases lipid cyclization, potentially affecting TEX_{86} accuracy. Here, we show that this "nutrient effect" is recorded in marine sediments and can be separated from the temperature signal. This effect may explain discrepancies between TEX_{86}-based temperature estimates and other proxies for surface ocean temperature, particularly in regions with strong nutrient variations. Accounting for nutrient effects is essential to improve TEX_{86} as a paleotemperature proxy.

1. Introduction

Reconstructing ocean temperatures is essential for understanding Earth's climatic history (Judd et al., 2024; Tierney et al., 2020). The paleotemperature proxy TEX_{86} (tetraether index of 86 carbons) is widely applied to reconstruct surface ocean temperatures throughout the Mesozoic–Cenozoic, particularly during greenhouse intervals (Judd et al., 2022). The proxy is based on the degree of cyclization of archaeal membrane lipids preserved in marine sediments. These lipids include isoprenoid glycerol dialkyl glycerol tetraethers (GDGTs) containing 0–3 cyclopentyl moieties (commonly referred as GDGT-*n*, where *n* denotes the number of internal rings), along with crenarchaeol (cren) and its isomer (cren')—two unique GDGTs with four cyclopentyl and one cyclohexyl moieties (Sinninghe Damsté et al., 2002). Warmer sea surface temperatures (SSTs) generally correspond to a higher proportion of cyclized GDGTs in surface (core-top) marine sediments, resulting in higher TEX_{86} values, as defined by Schouten et al. (2002):

$$TEX_{86} = \frac{[GDGT-2] + [GDGT-3] + [Cren']}{[GDGT-1] + [GDGT-2] + [GDGT-3] + [Cren']}$$

This relationship reflects homeoviscous adaptation, a physical mechanism where the degree of cyclization in archaeal membrane lipids adjusts to temperature. Experimental evidence, including (hyper)thermophilic (De Rosa et al., 1980; Uda et al., 2001) and mesophilic (Elling et al., 2015) archaeal cultures, as well as seawater mesocosms containing mixed marine archaeal populations (Schouten et al., 2007; Wuchter et al., 2004), strongly supports the use of TEX_{86} as a reliable paleothermometer.

Although core-top TEX_{86} correlates strongly with ocean surface temperatures, non-thermal factors such as archaeal community structure (Hurley et al., 2018; Rattanasriampaipong et al., 2022b; Taylor et al., 2013; van der Weijst et al., 2022; Villanueva et al., 2015) and biogeochemical conditions that impose energetic stress (Elling et al., 2014; Qin et al., 2015) also influence GDGT distributions. Notably, the role of nutrient availability remains

Methodology: Ronnakrit Rattanasriampaipong, Jessica E. Tierney, Jordan T. Abell
Resources: Jessica E. Tierney, Jordan T. Abell
Software: Ronnakrit Rattanasriampaipong
Supervision: Jessica E. Tierney
Validation: Jessica E. Tierney
Visualization: Ronnakrit Rattanasriampaipong
Writing – original draft: Ronnakrit Rattanasriampaipong
Writing – review & editing: Ronnakrit Rattanasriampaipong, Jessica E. Tierney, Jordan T. Abell

underexplored, despite laboratory evidence showing that archaeal growth under conditions with limited electron donors (i.e., limited substrate availability; Elling et al., 2014; Hurley et al., 2016; Evans et al., 2018) or acceptors (i.e., low oxygen conditions; Qin et al., 2015) can enhance GDGT cyclization in archeal cultures. Observations from both modern water columns (e.g., Hurley et al., 2018) and paleoclimate records (e.g., Junium et al., 2018; Polik et al., 2018) further suggest that nutrient availability may shape TEX_{86} signals, potentially through its influence on archeal metabolism and GDGT production.

Marine archaea are key ammonia oxidizers in today's oceans (Francis et al., 2005; Karner et al., 2001; Wuchter et al., 2006), playing a central role in ocean nitrification by converting ammonia to nitrite, which is subsequently oxidized to nitrate by nitrifying bacteria. The availability of these bioavailable nitrogen species regulates surface ocean productivity (Tyrrell, 1999; Yool et al., 2007) and influences archaeal metabolism (Martens-Habbena et al., 2009; Peng et al., 2016; Proctor et al., 2023; Ward, 2008, 2011). While direct indicators of archaeal ammonia oxidation, such as ammonia oxidation rates, ammonia/ammonium concentrations, or nitrite concentrations, would provide the best constraints on archaeal growth conditions (cf. Beman et al., 2008; Qin et al., 2015; Sintes et al., 2013; J. M. Smith et al., 2014; Wuchter et al., 2006), such measurements remain geographically sparse and lack global coverage (cf. Paulot et al., 2015; Tang et al., 2023). In contrast, nitrate—the final product of oceanic nitrification—is widely measured and provides an accessible alternative for assessing ammonia oxidation patterns.

Available data show a moderate yet significant correlation between ammonia oxidation rates and surface ocean nitrate concentrations ($\rho = 0.34$, $P < 0.001$; see Figure S1b in Supporting Information S1), suggesting a general link between ammonia oxidation and nitrate availability in surface oceans. However, this modest correlation reflects the complexity of the marine nitrogen cycle, where physical and biogeochemical factors can decouple ammonia/nitrite from nitrate (Sarmiento & Gruber, 2006). For example, in regions with strong nitrate supply—such as upwelling zones and river-influenced coastal waters—nitrate concentrations may broadly reflect physical transport rather than in situ nitrification, potentially masking low ammonia availability. Given the exploratory nature of our work, we use nitrate concentrations as a practical proxy for ammonia oxidation to investigate how nutrient availability influences marine archaeal TEX_{86} at a global scale, while acknowledging the complexity and potential decoupling in nitrate and ammonia/nitrite relationships, particularly near upwelling zones.

2. Data and Methods

2.1. Ocean Temperatures and Nitrate Concentrations

Although marine archaea inhabit the entire water column (Karner et al., 2001), the primary GDGT signals preserved in marine sediments are thought to originate predominantly from above the thermocline due to efficient export mechanisms via the biological pump (cf. Siegel et al., 2023; Zhang & Liu, 2018). The precise export depth range of GDGTs remains an active area of research (e.g., Hurley et al., 2018; Zhang & Liu, 2018), and previous calibration studies have proposed both sea surface and subsurface temperature reconstructions using TEX_{86} (e.g., J.-H. Kim et al., 2008, 2010; Tierney & Tingley, 2014, 2015b). To account for the habitat depth range of marine archaea while acknowledging the common application of TEX_{86} as a proxy for sea surface and subsurface temperatures, we use thermocline-integrated average temperature and nitrate concentrations.

To compute these values, we use the $0.25° \times 0.25°$ ocean temperature mean field (*t_mn*) from the 1991–2020 decadal average provided by the 2023 World Ocean Atlas (WOA23; Locarnini et al., 2024). The thermocline depth was determined as the depth at which the maximum rate of temperature change occurs in each spatial grid. We then calculated *thermocline-integrated average temperature* (hereafter *thermocline-integrated T or thermo-T*) by integrating ocean temperatures from the surface down to the determined thermocline depth and dividing by that depth. In this study, thermocline depths range from 50 to 400 m below sea level (Figure S2b in Supporting Information S1), reflecting spatial variability across the global ocean. Unlike previous subsurface temperature calibrations that assume a fixed upper-thermocline depth (e.g., 200 m in J.-H. Kim et al., 2012; Tierney & Tingley, 2015b), our approach captures local stratification differences (Figures S2g and S2h in Supporting Information S1). Consequently, relative to 0–200 m averages, thermo-T is generally warmer in upwelling regions and cooler in subtropical gyres than both gamma-weighted and linear-mean temperatures (Figures S2c–S2f in Supporting Information S1; cf. J.-H. Kim et al., 2012; Tierney & Tingley, 2015b).

Nitrate concentrations were derived from the Copernicus Marine Environment Monitoring Service (CMEMS) global ocean biogeochemistry hindcast product (Perruche, 2018). Decadal averages of nitrate concentrations were calculated from the 0.25° × 0.25° monthly mean fields spanning 1993–2022 using the *ncclimo* NetCDF Climatology Generator. We then re-gridded the CMEMS nitrate data set by interpolating to the spatial coordinates of the WOA23 temperature data set to ensure coordinate consistency (see Figure S3 in Supporting Information S1). As with ocean temperatures, we calculated a *thermocline-integrated nitrate* value (hereafter referred to as "*nitrate*").

2.2. Global TEX_{86} Core-Top Observations

We update the global core-top data set previously used in the Bayesian temperature calibration model BAYSPAR ($n = 1095$; Tierney & Tingley, 2014, 2015b). The updated data set includes 2,084 core-top TEX_{86} observations, incorporating:

1. Data published in previous compilation efforts (J.-H. Kim et al., 2008, 2010; Tierney & Tingley, 2014, 2015b),
2. data published in studies since 2015 (Ceccopieri et al., 2018; J. Chen et al., 2018; Hagemann et al., 2023; Harning et al., 2019, 2023; Jaeschke et al., 2017; Kaiser et al., 2015; J.-H. Kim et al., 2015, 2016; Kusch et al., 2016; Lamping et al., 2021; Lo et al., 2018; Pan et al., 2016; Richey & Tierney, 2016; Rodrigo-Gámiz et al., 2015; Schukies, 2018; Sinninghe Damsté, 2016; Sinninghe Damsté et al., 2022; Tierney et al., 2015; Varma, Hopmans, van Kemenade, et al., 2024; B. Wei et al., 2020; Y. Yang et al., 2018), and
3. new data ($n = 170$) analyzed for this study.

The spatial distribution of the updated database is shown in Figure S4 in Supporting Information S1. These data originate from multiple publications and laboratories with different analytical approaches. While protocols for GDGT determination using high performance liquid chromatography (HPLC)–mass spectrometry (MS) have evolved over the years, we specify the method used whenever available. However, previous work suggests that older and newer HPLC-MS methods produce comparable results (cf. Hopmans et al., 2016, see Text S1 in Supporting Information S1 for details). We removed samples that are heavily impacted by non-pelagic GDGT sources, based on thresholds of the Branched versus Isoprenoid Tetraether (BIT) index >0.5 (terrestrial GDGT inputs; Hopmans et al., 2004; Weijers et al., 2006), Methane Index >0.5 (GDGT inputs from methanotrophs; B. Kim & Zhang, 2023; Zhang et al., 2011), and %GDGT-0 >60 (GDGT inputs from methanogens; Blaga et al., 2009; Inglis et al., 2015; Sinninghe Damsté et al., 2012).

The dominant environmental influence on core-top TEX_{86} is ocean temperature (J.-H. Kim et al., 2008, 2010; Schouten et al., 2002; Tierney & Tingley, 2014, 2015b). To ensure spatial consistency, core-top TEX_{86} observations were mapped onto a uniform 0.25° × 0.25° grid, with median values representing grid cells containing multiple observations. A simple linear regression of the updated database indicates that thermocline-integrated temperatures explain 76% ($r^2 = 0.76$) of the TEX_{86} variance (Figure 1a). This regression is not intended as a new subsurface calibration but is instead used to isolate the dominant thermal effect in order to evaluate the secondary influence of nutrients. TEX_{86} residuals were calculated by subtracting predicted TEX_{86} from observed values. Following J.-H. Kim et al. (2010) and Tierney and Tingley (2014, 2015b), core-top TEX_{86} from high-latitude sites (>70°N) were excluded from the linear regression, as TEX_{86} values from the high Arctic region do not show sensitivity to ocean surface temperatures.

3. Results and Discussion

3.1. A Nutrient Effect on Marine Sedimentary TEX_{86}

Core-top TEX_{86} residuals exhibit a weak but statistically significant negative correlation with the logarithm of nitrate concentrations (Spearman's $\rho = -0.17$, $P < 0.001$; Figure 1b). This weak global correlation highlights the complexity of sources and sinks of marine nitrogen species, and potentially reflects regions where ammonia and nitrate concentrations are decoupled. Additionally, residual variability may be influenced by other known factors, such as water depth, as well as unidentified sources of noise that affect TEX_{86}. A stronger relationship emerges when we restrict the regression to low-nutrient environments, defined as nitrate concentrations below 2.7 μmol/L ($\rho = -0.33$, $P < 0.001$; Figure 1b). The low-nutrient threshold corresponds to the nitrate concentration at which the rolling mean of TEX_{86} residuals, calculated using a sliding window of 19 data points, reaches its minimum.

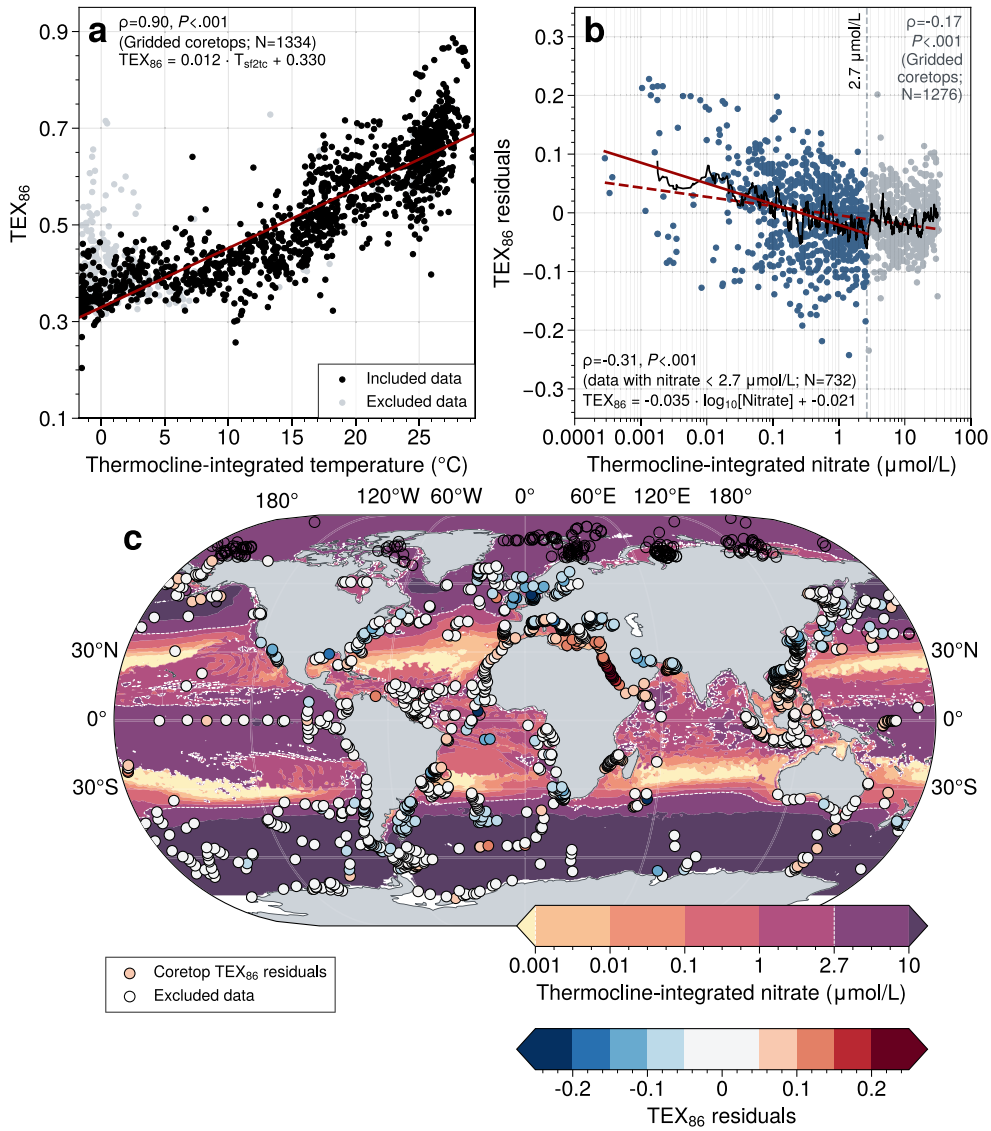

Figure 1. Positive TEX_{86} residuals in surface marine sediments correspond to low-nutrient regions. (a) The correlation between gridded core-top TEX_{86} values and thermocline-integrated ocean temperature. Data north of 70°N were excluded from the regression following J.-H. Kim et al. (2010) and Tierney and Tingley (2014, 2015b). (b) TEX_{86} residuals (observed—predicted) from the temperature regression in panel (a) show a weak but significant negative correlation with nitrate concentrations, suggesting a "nutrient effect." This effect is more pronounced in low-nutrient regions (highlighted in blue), defined by a threshold of 2.7 µmol/L, where the lowest rolling mean of TEX_{86} residuals is observed. The solid black line represents the rolling mean, calculated using a sliding window of 19 data points. (c) Spatial distribution of gridded core-top TEX_{86} residuals, with higher values generally occurring in regions with low nitrate concentrations. Shaded contours indicate nitrate levels, with the low-nutrient threshold contour of 2.7 µmol/L (white dashed line).

We tested different window sizes in the range [5, 100] and selected the one that yielded the strongest correlation between nitrate and TEX_{86} residuals (see Figure S5 in Supporting Information S1).

We isolated the correlation between TEX_{86} residuals and nitrate using a linear fit for simplicity; however, an exponential fit yields similar results (see Column 2 in Figure S6 in Supporting Information S1). When we explore residuals using existing subsurface calibrations, we find that the BAYSPAR model of Tierney and Tingley (2014, 2015b) largely suppresses this nutrient effect. This is due to BAYSPAR's regionally adjusted slopes and intercepts of a linear fit, which reduce systematic global residual patterns—resulting in no discernible correlation between residuals and nitrate (see Column 3 in Figure S6 in Supporting Information S1). In contrast, the TEX_{86}^{H}-subT calibration of J.-H. Kim et al. (2012), when applied to the global core-top data set, produces strong structure in

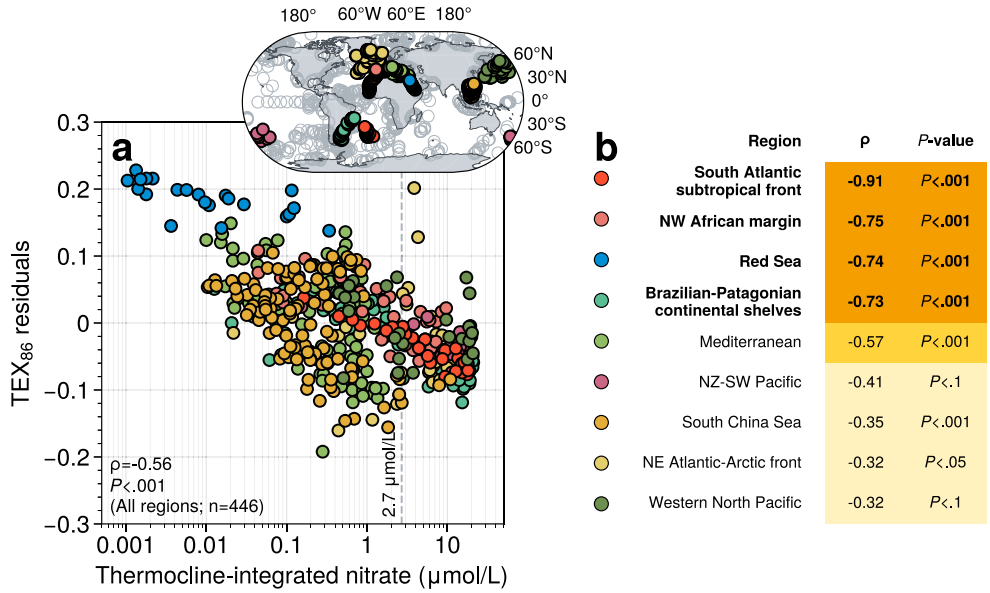

Figure 2. A pronounced nutrient effect on core-top TEX_{86} in regions with strong horizontal nutrient gradients. (a) Scatter plot illustrating the relationship between regional gridded core-top TEX_{86} residuals and nitrate concentrations, with an overall Spearman correlation coefficient ($\rho = -0.56$; $P < 0.001$; $n = 446$). The vertical dash line shows the low-nutrient threshold of 2.7 µmol/L. An inset map showing core-top locations of regions with significant negative correlations between TEX_{86} residuals and NO_3^- concentrations. (b) Spearman correlation coefficients (ρ) and associated *P*-values for specific regions, with the corresponding colored markers displayed before each region name.

TEX_{86} residuals versus thermo-T due to regression dilution that somewhat mask the effect (see Column 4 in Figure S6 in Supporting Information S1).

While ammonia availability regulates the cellular metabolism of marine archaea (Peng et al., 2016; Proctor et al., 2023; Ward, 2008, 2011), our findings suggest that nitrate is a reasonable proxy for identifying low-nutrient (low-ammonia) locations. The observed relationship between TEX_{86} residuals and nitrate indicates that archaeal communities grow more slowly (i.e., exhibit lower ammonia oxidation rates) in regions with low nutrients, and produce GDGTs with more rings, leading to higher TEX_{86}. This trend aligns with laboratory experiments showing that archaea decrease membrane permeability by synthesizing GDGTs with higher ring numbers under energy-limiting conditions (Elling et al., 2015; Evans et al., 2018; Hurley et al., 2016). The magnitude of elevated TEX_{86} of about 0.1 proxy units at the lowest values of nitrate agrees well with experimental evidence (Hurley et al., 2016). Given the logarithmic nature of the regression, the effect of nitrate limitation spans a concentration range of 0.0003–2.7 µmol/L. For context, nitrate levels between 0.5 and 2 µmol/L are considered limiting for primary productivity in the surface ocean (e.g., Browning & Moore, 2023; Henley et al., 2020).

To further investigate this nutrient effect, we analyzed regional-scale patterns, focusing on areas that have large horizontal nutrient gradients and where core-top TEX_{86} residuals show a strong negative correlation with nitrate. TEX_{86} residuals from these regions show an average negative correlation with nitrate of $\rho = -0.56$ ($P < 0.001$; Figure 2a), with core-tops near the South Atlantic Subtropical Front exhibiting the strongest relationship ($\rho = -0.91$, $P < 0.001$; Figure 2b). Notably, TEX_{86} residuals from the Red Sea show a strong nutrient effect ($\rho = -0.74$, $P < 0.001$; Figure 2b). This contrasts with the original study of sedimentary TEX_{86} in the Red Sea, which found no strong correlation between TEX_{86} and nitrate concentrations at 100 m depth (Trommer et al., 2009). We attribute this discrepancy to three factors. First, the WOA nitrate fields are on a coarse $1° \times 1°$ grid with a relatively high minimum concentration, which smooths out the steep, localized nutrient gradients of the Red Sea. Second, relying on a single fixed 100 m depth ignores spatial variability in thermocline depth and near-surface nutrient distributions in this restricted basin. Third, the original study correlated raw TEX_{86} values with nitrate without removing the confounding thermal effect, whereas our use of TEX_{86} residuals isolates the potential nutrient signal. These choices mask the fine-scale biogeochemical variability that emerges when using higher-resolution CMEMS data and thermocline-integrated nitrate (see Figure S7 in Supporting Information S1).

While earlier studies attributed anomalously high TEX_{86} in the Red Sea to endemic clades of marine archaea (J.-H. Kim et al., 2010; Trommer et al., 2009), our findings suggest a more parsimonious explanation: elevated TEX_{86} reflects extreme nutrient stress in this oligotrophic sea.

3.2. Implications for TEX_{86} Paleothermometry

TEX_{86}–derived ocean temperature estimates occasionally yield anomalously high values that diverge from other proxies and paleoclimate expectations. Here, we explore two paleoclimate scenarios in which nutrient stress may account for the discrepancies between TEX_{86}-derived temperatures and SST estimates from the $U^{K'}_{37}$ proxy—an independent organic paleotemperature proxy based on unsaturated ketones produced by coccolithophores (Brassell et al., 1986; Prahl & Wakeham, 1987). Although multiple calibrations for TEX_{86} exist, some of which are non-linear (J.-H. Kim et al., 2010), in these examples we convert TEX_{86} to temperatures using the simple linear regression with thermocline-integrated T developed above to highlight deviations from the general linear thermal effect. For the $U^{K'}_{37}$ data, we use the Bayesian calibration BAYSPLINE (Tierney & Tingley, 2018), which is linear up to temperatures of 25°C, at which point the proxy has a non-linear response as it approaches the maximum possible value of 1.

3.2.1. Denitrification Dynamics in the Arabian Sea Upwelling Zone

Reconstructed ocean temperatures from $U^{K'}_{37}$ and TEX_{86} records in the Arabian Sea capture the overall warming trend since the last deglaciation, marking the transition from the Last Glacial Maximum to the Holocene interglacial (Figure 3; Huguet et al., 2006; Tierney et al., 2016). A notable feature, however, is that TEX_{86}-derived temperatures are consistently warmer and more variable than $U^{K'}_{37}$-based SSTs throughout most of the past 20,000 years (Figure 3b). Furthermore, the thermocline-integrated temperatures exceeding 30°C during the Holocene, as suggested by TEX_{86}, are likely unrealistic given that modern-day SSTs in this region average approximately 26–27°C. This indicates additional factors contributing to TEX_{86} signals on top of seawater temperatures.

A particularly striking feature is the deviation in paleo-temperature proxies found during the Younger Dryas (YD, ca. 12.9–11.7 thousand years ago, ka; Rasmussen et al., 2006) and Heinrich Stadial 1 (HS1, ca. 17.5–14.5 ka; Broecker & Barker, 2007; McManus et al., 2004) events. During these intervals, TEX_{86}-derived temperatures increase sharply, whereas $U^{K'}_{37}$-based SSTs do not record warming (Figure 3b; Huguet et al., 2006; Tierney et al., 2016). In fact, both the $U^{K'}_{37}$ records and the TraCE-21ka paleoclimate model simulation—a fully coupled simulation of Transient Climate Evolution over the past 21,000 years—indicate surface cooling during the YD and HS1, reflecting broader Northern Hemisphere climate dynamics (Huguet et al., 2006; Schulte & Müller, 2001; Sonzogni et al., 1998; Tierney et al., 2016). While Tierney et al. (2016) attributed this discrepancy to TEX_{86} recording subsurface water warming, the magnitude of the TEX_{86} warming anomalies—up to 7°C from the pre-event baseline (Figure 3b)—is unrealistically large. Together, these observations suggest that TEX_{86} is influenced by additional environmental factors beyond temperature alone.

Core sites NIOP-C2_905_PC and SO42-74KL are located in the Arabian Sea, where nitrate concentrations are generally low. However, these sites lie at the periphery of present-day high-nutrient "blobs" (Figure 3d), making them particularly sensitive to spatial and temporal variations in nutrient dynamics. Under today's interglacial conditions, the high-nutrient "blobs" persist in this region, potentially supplying nutrients to these sites. However, this feature may have dissipated during past cooling episodes. Weakened monsoon winds during the YD and HS1 (Tierney et al., 2016) likely reduced upwelling, limiting the supply of nutrient-rich waters to the surface. This could have induced relatively stronger nutrient stress in marine archaea, leading to the production of more cyclic GDGTs and higher TEX_{86} values.

This interpretation is supported by denitrification proxy records from these two sites. Lower bulk sediment $\delta^{15}N$ values during the YD and HS1 indicate reduced denitrification, consistent with weakened upwelling and lower nitrate availability in surface waters (Figure 3c; Altabet et al., 1995, 2002; Ivanochko et al., 2005; Suthhof et al., 2001). Moreover, after interpolating all time series ($U^{K'}_{37}$, TEX_{86}, and $\delta^{15}N$) onto a common time step, we find that TEX_{86} T anomalies (Thermo - $T_{TEX_{86}}$ - $SST_{U^{K'}_{37}}$) exhibit a strong negative correlation with bulk sediment

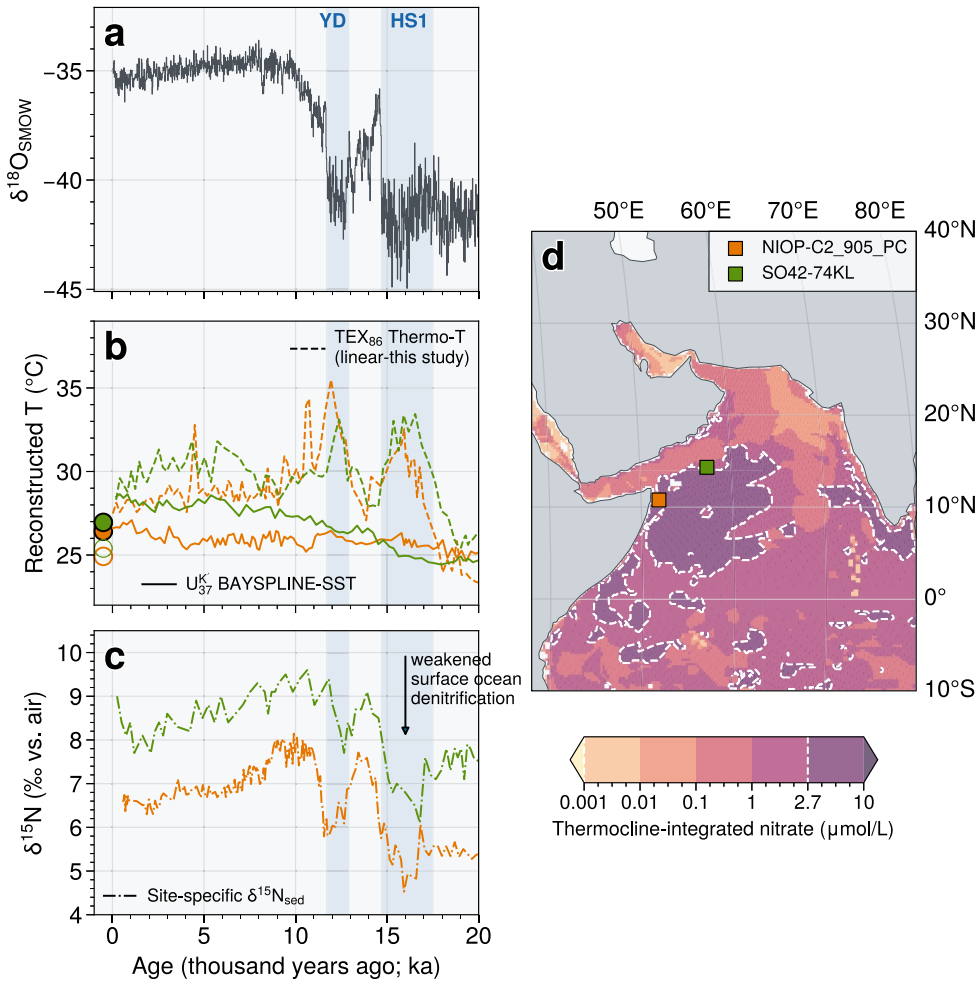

Figure 3. Anomalously warm TEX_{86} signals during the Younger Dryas (YD) and Heinrich Stadial 1 (HS1) in the Arabian Sea. (a) Northern Greenland Ice Project (NGRIP) ice core $\delta^{18}O$ record (Seierstad et al., 2014), highlighting cooling during YD (ca. 12.9–11.7 kyr BP; Rasmussen et al., 2006) and HS1 (ca. 17.5–14.5 kyr BP; Broecker & Barker, 2007; McManus et al., 2004). (b) Reconstructed ocean temperatures from sediment cores NIOP-C2_905_PC and SO42-74KL in the Arabian Sea. $U^{K'}_{37}$-derived sea surface temperature (SST) records are based on the BAYSPLINE calibration (Tierney & Tingley, 2018), while TEX_{86}-derived thermocline-integrated temperatures (thermo-T) are based on the linear regression of the updated core-top data set (see Figure 1a). Original proxy data were retrieved from Huguet et al. (2006). Modern SST (filled circles) and thermo-T (open circles) are indicated. (c) Bulk sediment $\delta^{15}N$ records from NIOP-C2_905_PC (Ivanochko et al., 2005) and SO42-74KL (Suthhof et al., 2001), serving as a proxy for surface ocean denitrification. The records indicate reduced denitrification during cooling events. Data sourced from the global ocean nitrogen isotope database (Tesdal et al., 2013). (d) A map showing nitrate concentrations with core locations. White dashed contours highlights regions with elevated nitrate concentrations (>2.7 µmol/L surface nitrate) within the overall low-nutrient background of the Arabian Sea.

$\delta^{15}N$ during the YD and HS1 (see Figures S8a and S8b in Supporting Information S1). By subtracting the Holocene mean values from the TEX_{86} records, we de-trend the data and find that temperature anomalies of up to 7°C correspond to increases of up to 0.1 proxy units in TEX_{86} (see Figures S8c and S8d in Supporting Information S1), which is similar to the magnitude observed in the modern core-top records discussed above.

Collectively, these lines of evidence suggest that TEX_{86} temperatures in the Arabian Sea are sensitive to nutrient availability in surface waters. Reduced upwelling during the YD and HS1 events likely amplified the nutrient stress on marine archaea, resulting in anomalously high TEX_{86} values. It is important to note that we do not observe a comparable TEX_{86} warming anomaly during the Last Glacial Maximum (LGM, ca. 20–19 ka; Clark et al., 2009) in spite of low $\delta^{15}N$ values. This suggests that surface ocean circulation patterns, monsoonal

dynamics, and nutrient availability in this region differed between the nearly steady-state conditions of the LGM and the transient cooling events of the deglacial period.

3.2.2. South Pacific Subtropical Gyre Poleward Expansion

Our second example investigates ocean temperature changes in the Tasman Sea, a region that harbors a strong north-south nutrient gradient in the present day (see Figure 4d). Over the past 150,000 years, $U^{K'}_{37}$ and TEX_{86} temperatures largely track each other, reflecting the broader global climate history since the penultimate deglaciation (Figure 4). However, TEX_{86}-derived temperatures occasionally exceed 25°C—an implausibly high value given the modern SSTs at these core sites range from 18 to 21°C. This discrepancy suggests that factors beyond temperature influence the proxy.

Today, DSDP Site 591 (31°35.06′S; 164°26.92′E; 2,131 m water depth) is located within the Tasman Front, which is a component of the low-nutrient western boundary of the South Pacific Subtropical Gyre (SPSTG). IODP Site U1510 (36°19.7385′S, 164°33.5220′E; 1,238 m water depth), while still within the gyre's low-nutrient

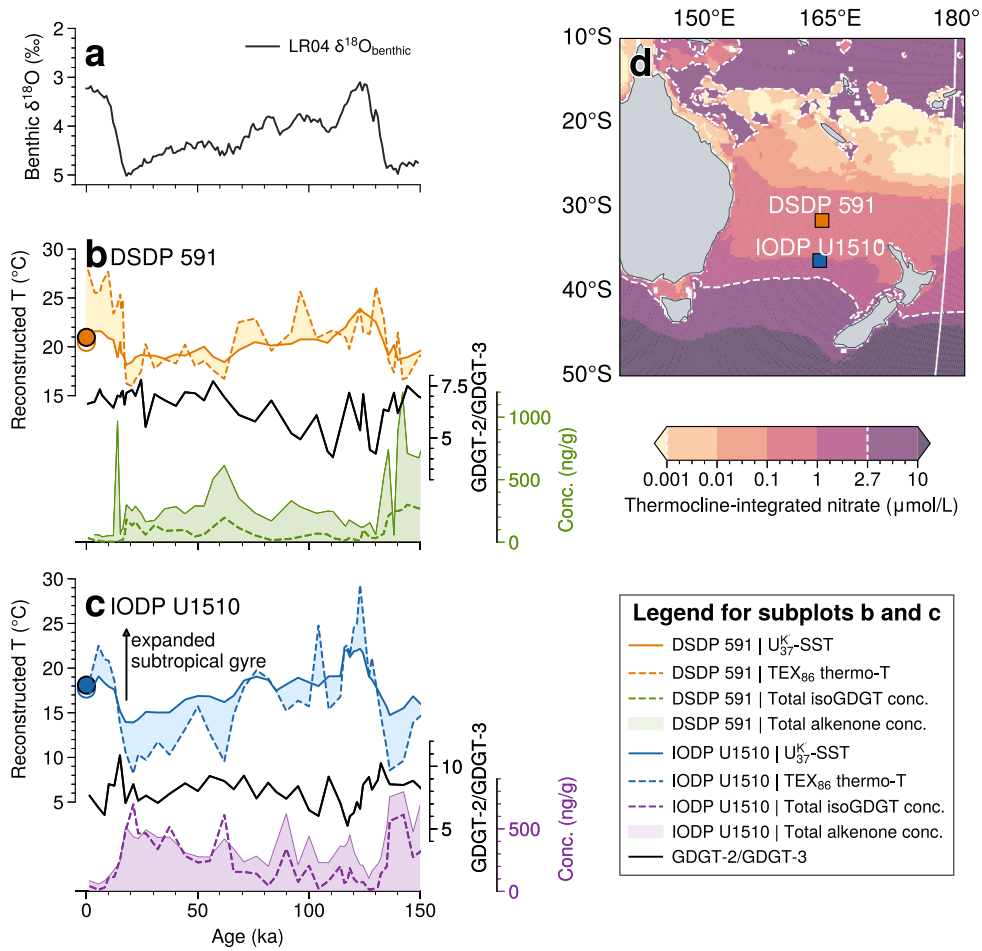

Figure 4. Nutrient effects on TEX_{86} records in the Tasman Sea. (a) LR04 global benthic foraminiferal $\delta^{18}O$ stack (Lisiecki & Raymo, 2005), representing climate variability across glacial-interglacial cycles since the penultimate deglaciation (ca. 138 ka; Govin et al., 2015). (b) Reconstructed ocean temperatures at DSDP 591. $U^{K'}_{37}$-derived sea surface temperatures (SST; solid) are based on the BAYSPLINE calibration (Tierney & Tingley, 2018), while TEX_{86}-derived thermocline-integrated temperatures (thermo-T; dashed) are based on the linear regression from this study (see Figure 1a). Modern SST (filled circle) and thermo-T (open circle) are shown for reference. GDGT-2/GDGT-3 (black), total alkenone (filled) and isoGDGT concentrations (dashed) are also plotted. (c) Same as (b), but for IODP U1510. (d) A map showing core locations in the Tasman Sea. Shaded contours represent modern nitrate concentrations. The white dashed contour marks the low-nutrient core (<2.7 µmol/L surface nitrate) of the South Pacific Subtropical Gyre.

zone, is positioned approximately 5° further south, where surface waters are impacted primarily by eddies shed from the East Australian Current (Ganachaud et al., 2014; Sloyan & O'Kane, 2015; Talley et al., 2011). Core-top TEX_{86} residuals from the adjacent southwest Pacific (see the NZ-SW Pacific region in Figure 2) also exhibit a pronounced nutrient effect.

Visual inspection reveals episodic warming events in which TEX_{86}-derived temperatures temporarily exceed $U^{K'}_{37}$-based SSTs. These events generally occur during globally-warmer periods (Figures 4a–4c). Conversely, during colder intervals TEX_{86} temperatures are typically lower than $U^{K'}_{37}$-based SSTs, suggesting that the proxies are either representing different depth habitats (with $U^{K'}_{37}$ representing the surface and TEX_{86} the thermocline) or different seasons (e.g., $U^{K'}_{37}$ represents the warmer season).

Total C_{37} alkenone concentrations, indicative of haptophyte productivity, largely follow glacial-interglacial (G-IG) cycles, with elevated concentrations during glacial intervals and lower concentrations during interglacials (see Figures 4b and 4c). Total isoprenoid GDGT (isoGDGT) concentrations follow a similar pattern. Although marine archaea inhabit the entire water column (Karner et al., 2001), we interpret isoGDGT concentrations in our records as reflecting archaeal productivity in the upper water column due to (a) their parallel variations with alkenone concentrations, and (b) the absence of exogenous GDGT sources (reflected by their low BIT, MI, and % GDGT-0 indices; see Data Set S7).

We suggest that the extreme warmth in TEX_{86} temperatures during interglacials reflects changes in surface nutrient availability driven by enhanced upper-ocean stratification, the poleward expansion of the SPSTG, or a combination of both mechanisms. A first-order observation is that biomarker concentrations are generally higher and closely track G-IG cycles at IODP Site U1510, whereas at DSDP Site 591, concentrations are overall lower, with episodic spikes of high alkenone concentrations near deglacial periods. Located near the nutrient-depleted core of the subtropical gyre, DSDP Site 591 may have experienced less variability, especially during prolonged interglacial conditions. In contrast IODP Site U1510, located near a dynamic nutrient-rich frontal boundary, likely experienced greater variability in nutrient supply and primary productivity through time. Correlations between temperature anomalies (Thermo - $T_{TEX_{86}}$ - $SST_{U^{K'}_{37}}$) and biomarker concentrations further support these proposed interpretations (see Figure S9 in Supporting Information S1). Assuming alkenone and isoGDGT concentrations reflect export productivity and in turn nutrient availability, these results suggest that nutrient stress during interglacials results in elevated TEX_{86}. Stronger correlations at IODP Site U1510 ($\rho = -0.68$ for alkenones, $\rho = -0.82$ for isoGDGTs, both $P < 0.001$) compared to DSDP Site 591 ($\rho = -0.31$, $P<.05$ for alkenones and $\rho = -0.62$, $P < 0.001$ for isoGDGTs) likely reflects differences in how much the surface nutrient availability is changing through glacial-interglacial cycles at each site. Comparisons between the biomarker concentrations and the benthic foraminiferal $\delta^{18}O$ stack also support this; with a stronger correlation at IODP Site U1510 (see Figure S10 in Supporting Information S1).

Although GDGT-2/GDGT-3 values at both sites are moderately high—above the conventional threshold of <5—suggesting contributions from deep-water marine archaea (cf. Rattanasriampaipong et al., 2022b; Taylor et al., 2013), their temporal variations may reflect changes in surface ocean stratification. GDGT-2/GDGT-3 generally anti-correlate with Thermo - $T_{TEX_{86}}$, with two pronounced minima during the last interglacial (ca. 100–130 ka) coinciding with peak Thermo - $T_{TEX_{86}}$ (Figures 4b and 4c). These low GDGT-2/GDGT-3 values may indicate reduced input from deep-water clades during nutrient-poor, warm intervals, when deep-dwelling chemoautotrophs are nutrient-limited. GDGT-2/GDGT-3 and Thermo - $T_{TEX_{86}}$ show weak but significant correlations at both sites (Figures S10e and S10f in Supporting Information S1). Though this relationship is likely confounded by thermal effects, it emphasizes the need to disentangle temperature and nutrient influences in TEX_{86} interpretations.

Modern observations indicate that warming and weaker winds promote increased stratification in the Tasman Sea's upper ocean layers, a phenomenon evident from satellite ocean color and altimetry data (cf. Tilburg et al., 2002). Paleoclimate reconstructions further suggest poleward migration of the Tasman Front (Kawagata, 2001; Martínez, 1994) and the Subtropical Front in the southwest Pacific (Bostock et al., 2015; Hayward et al., 2012; Sikes et al., 2009) during warmer periods of the late Quaternary. Model simulations also indicate that warming leads to the expansion of subtropical gyres (Polovina et al., 2011; H. Yang et al., 2020), a process that can intensify oligotrophic conditions at these sites. In our view, whether stratification increases primarily due to

thermal effects, front migration, or gyre expansion, the outcome is a reduction in nutrient availability at the surface in the Tasman Sea. This nutrient limitation could trigger physiological shifts in marine archaea—altering GDGT production and distribution—and ultimately lead to an overestimation of TEX_{86}-based temperatures during warmer intervals of the last 150,000 years.

4. Conclusions

Our study demonstrates that a "nutrient effect" is recorded in sedimentary TEX_{86}, wherein low-nutrient regions of the global ocean are associated with higher TEX_{86} values. This observation is consistent with laboratory studies showing that nutrient limitation leads to higher GDGT cyclization (Elling et al., 2014; Hurley et al., 2016), and the magnitude of increased cyclization observed in modern environments aligns well with experimental evidence (Hurley et al., 2016). Furthermore, comparisons between TEX_{86} and $U_{37}^{K'}$ paleotemperature reconstructions in the Arabian Sea and Tasman Sea indicate that nutrient stress likely influenced GDGT distributions during the last glacial-interglacial cycle, albeit with region-specific signatures. This nutrient effect offers a plausible explanation for the commonly observed higher variance in TEX_{86}-based temperature reconstructions relative to $U_{37}^{K'}$, as reported in both isoprenoid GDGT studies (e.g., bin Shaari et al., 2013; Caley et al., 2011; Ho & Laepple, 2015, 2016) and those incorporating hydroxylated GDGTs (OH-GDGTs; cf. Fietz et al., 2016).

Our results suggest that previous TEX_{86}-based temperature reconstructions—especially for warm climate intervals—may require reevaluation. Integrating TEX_{86} with independent proxies such as $\delta^{15}N$ and paleo-productivity markers could help resolve discrepancies among proxies and between proxy data and climate model simulations—e.g., during the early Eocene (Hollis et al., 2019). Nutrient stress may also explain extreme TEX_{86} values in deep-time hyperthermal events such as the Paleocene-Eocene Thermal Maximum (cf. Zachos et al., 2001, 2008) and Ocean Anoxic Events (cf. Kuypers et al., 2001; van Helmond et al., 2014). During these intervals, increased weathering likely supplied nutrients to coastal oceans, but intensified warming and stronger upper-ocean stratification restricted vertical nutrient supply in the open ocean (Erbacher et al., 2001). This could have led to lower concentrations of important nitrogen species, enhanced nutrient stress on marine archaea, and overproduction of cyclic GDGTs, resulting in anomalously high TEX_{86} values (>0.8) (e.g., Forster, Schouten, Baas, & Sinninghe Damsté, 2007; Forster, Schouten, Moriya, et al., 2007; Sinninghe Damsté et al., 2010). Our findings highlight the importance of considering nutrient stress when interpreting TEX_{86} signals in both recent and deep-time climate reconstructions.

Recognizing the dual influence of temperature and nutrient availability on GDGT production is crucial for improving TEX_{86}-based paleotemperature reconstructions. Future studies should quantify nutrient effects on GDGT cyclization across diverse archaeal clades via controlled culture experiments—similar to those reported by Hurley et al. (2016)—to further elucidate the mechanisms driving GDGT production. Additional core-top TEX_{86} observations in regions with pronounced nutrient gradients will help refine proxy calibrations. However, as nitrate concentrations can become decoupled from ammonia and nitrite—particularly in upwelling regions—future studies would benefit from globally distributed measurements of ammonia and nitrite to better constrain nutrient-driven variations in TEX_{86}. Furthermore, we encourage future research to utilize high-resolution ocean data products whenever available, as low-resolution oceanographic data sets may fail to capture fine-scale nutrient gradients. As ongoing warming alters ocean stratification and nutrient distributions, explicitly incorporating nutrient effects into TEX_{86} calibrations will improve the accuracy of both past climate reconstructions and future projections, thereby enhancing the reliability of TEX_{86} as a paleotemperature proxy.

Data Availability Statement

In this study, we update the core-top TEX_{86} data set by integrating previous calibration compilations (Hagemann et al., 2023; J.-H. Kim et al., 2008, 2010; Tierney & Tingley, 2014, 2015b; Varma, Hopmans, van Kemenda, et al., 2024). Table S1 in Supporting Information S1 summarize the full list of previous works that published core-top GDGT data sets, including (a) data from original sources (Ceccopieri et al., 2018; J. Chen et al., 2018; Hagemann et al., 2023; Harning et al., 2019, 2023; Kusch et al., 2016; Liu et al., 2014; Richey & Tierney, 2016; Rodrigo-Gámiz et al., 2015; Schukies, 2018; Tierney & Tingley, 2014, 2015b; Tierney et al., 2015; Varma, Hopmans, van Kemenda, et al., 2024; B. Wei et al., 2020), (b) data sets available via NOAA-NCEI of Tierney and Tingley (2015a) (Castañeda et al., 2010; Chazen, 2011; W. Chen et al., 2014; Fallet et al., 2012; Hernández-

Sánchez et al., 2014; Ho et al., 2011, 2014; Hu et al., 2012; Jia et al., 2012; Kaiser et al., 2014; J.-H. Kim et al., 2008, 2010; Leider et al., 2010; Lengger et al., 2014; Lü et al., 2014; Nieto-Moreno et al., 2013; Park et al., 2014; Richey et al., 2011; Seki et al., 2009, 2014; Shevenell et al., 2011; M. Smith et al., 2013; Trommer et al., 2009; Verleye, 2011; Y. Wei et al., 2011; Wu et al., 2012; Zell et al., 2014; Zhou et al., 2014), (c) data sets available via Figshare of Rattanasriampaipong et al. (2022a) (J.-H. Kim et al., 2015, 2016; Pan et al., 2016), (d) data sets available via PANGAEA of Hagemann et al. (2023) (Jaeschke et al., 2017; Kaiser et al., 2015; Lamping et al., 2021), and data sets available via PANGAEA of Varma, Hopmans, van Kemenda, et al. (2024) (Bale et al., 2013; Lo et al., 2018; Sinninghe Damsté, 2016; Sinninghe Damsté et al., 2022; Y. Yang et al., 2018).

This research used samples and/or data (Sample request IDs: 090658IODP, 094390IODP, 094429IODP, and 099796IODP) provided by the International Ocean Discovery Program (IODP). These samples are from DSDP Site 591 (Kennett & Borch, 1986; Tilburg et al., 2001) and IODP Site U1510 (Sutherland et al., 2019). The original age model for DSDP 591 was based on a comparison between planktic foraminifera (Martínez, 1994, 1997) and planktic foraminiferal oxygen isotopes (C. Nelson et al., 1994; C. S. Nelson et al., 1993). For Site U1510, the preliminary age model was based on a comparison between color reflectance data with the LR04 bethic stack (Lisiecki & Raymo, 2005). We updated age models of both sites using additional tie points based on alkenone-derived SSTs. See detailed in Text S2 in Supporting Information S1.

All geochemical proxy data sets, ocean data products, and analysis codes needed to reproduce our results are publicly accessible on Zenodo (https://doi.org/10.5281/zenodo.14806961; Rattanasriampaipong et al., 2025) and GitHub (https://github.com/PaleoLipidRR/nutrient-effect-on-TEX). The analyses were performed using Python 3.10 (Python 3.10, 2010) with key libraries including NumPy (Harris et al., 2020), Pandas (McKinney, 2010), and Xarray (Hoyer & Hamman, 2017). Statistical work utilized SciPy (Virtanen et al., 2020) and scikit-learn (Pedregosa et al., 2011), while figures were generated using Matplotlib (Hunter, 2007) and enhanced with the Proplot wrapper (https://proplot.readthedocs.io/en/stable/). A complete list of dependencies is provided in an exported. yml file in the GitHub repository.

We also used data from the EU Copernicus Marine Service Information's Global Ocean Biogeochemistry Hindcast product (https://doi.org/10.48670/moi-00019), ocean temperature data from the 2023 World Ocean Atlas (Locarnini et al., 2024), and data sets from the global nitrification (Tang et al., 2023) and ocean nitrogen isotope databases (Tesdal et al., 2013).

Acknowledgments

We thank the captains, chief scientists, and operational crews of DSDP Expedition 90 and IODP Expedition 371, as well as Kochi Core Repository staff who made marine sediment samples available for this research. This work was supported by the NOAA Climate and Global Change Postdoctoral Fellowship Program, administered by UCAR's Cooperative Programs for the Advancement of Earth System Science (CPAESS) under the NOAA Science Collaboration Program award (Grant number #NA23OAR4310383B) to R.R. This work was also supported by a National Science Foundation Ocean Sciences (NSF-OCE) Postdoctoral Research Fellowship (PRF) (award number #2126500) to J.T.A. J.E.T. acknowledges support from the David and Lucile Packard Fellowship in Science and Engineering and the Thomas R. Brown Distinguished Chair in Integrative Science. Finally, we thank the two anonymous reviewers whose comments improved the manuscript.

References

Altabet, M. A., Francois, R., Murray, D. W., & Prell, W. L. (1995). Climate-related variations in denitrification in the Arabian Sea from sediment $^{15}N/^{14}N$ ratios. *Nature*, *373*(6514), 506–509. https://doi.org/10.1038/373506a0

Altabet, M. A., Higginson, M. J., & Murray, D. W. (2002). The effect of millennial-scale changes in Arabian Sea denitrification on atmospheric CO_2. *Nature*, *415*(6868), 159–162. https://doi.org/10.1038/415159a

Bale, N. J., Villanueva, L., Hopmans, E. C., Schouten, S., & Sinninghe Damsté, J. S. (2013). Different seasonality of pelagic and benthic Thaumarchaeota in the North Sea. *Biogeosciences*, *10*(11), 7195–7206. https://doi.org/10.5194/bg-10-7195-2013

Beman, J. M., Popp, B. N., & Francis, C. A. (2008). Molecular and biogeochemical evidence for ammonia oxidation by marine Crenarchaeota in the Gulf of California. *The ISME Journal*, *2*(4), 429–441. https://doi.org/10.1038/ismej.2007.118

bin Shaari, H., Yamamoto, M., & Irino, T. (2013). Enhanced upwelling in the eastern equatorial Pacific at the last five glacial terminations. *Palaeogeography, Palaeoclimatology, Palaeoecology*, *386*, 8–15. https://doi.org/10.1016/j.palaeo.2013.03.022

Blaga, C. I., Reichart, G.-J., Heiri, O., & Sinninghe Damsté, J. S. (2009). Tetraether membrane lipid distributions in water-column particulate matter and sediments: A study of 47 European lakes along a north–south transect. *Journal of Paleolimnology*, *41*(3), 523–540. https://doi.org/10.1007/s10933-008-9242-2

Bostock, H. C., Hayward, B. W., Neil, H. L., Sabaa, A. T., & Scott, G. H. (2015). Changes in the position of the Subtropical Front south of New Zealand since the last glacial period. *Paleoceanography*, *30*(7), 824–844. https://doi.org/10.1002/2014PA002652

Brassell, S. C., Eglinton, G., Marlowe, I. T., Pflaumann, U., & Sarnthein, M. (1986). Molecular stratigraphy: A new tool for climatic assessment. *Nature*, *320*(6058), 129–133. https://doi.org/10.1038/320129a0

Broecker, W., & Barker, S. (2007). A 190‰ drop in atmosphere's $\Delta^{14}C$ during the "Mystery Interval" (17.5 to 14.5 kyr). *Earth and Planetary Science Letters*, *256*(1), 90–99. https://doi.org/10.1016/j.epsl.2007.01.015

Browning, T. J., & Moore, C. M. (2023). Global analysis of ocean phytoplankton nutrient limitation reveals high prevalence of co-limitation. *Nature Communications*, *14*(1), 5014. https://doi.org/10.1038/s41467-023-40774-0

Caley, T., Kim, J.-H., Malaizé, B., Giraudeau, J., Laepple, T., Caillon, N., et al. (2011). High-latitude obliquity as a dominant forcing in the Agulhas current system. *Climate of the Past*, *7*(4), 1285–1296. https://doi.org/10.5194/cp-7-1285-2011

Castañeda, I. S., Schefuß, E., Pätzold, J., Sinninghe Damsté, J. S., Weldeab, S., & Schouten, S. (2010). Millennial-scale sea surface temperature changes in the eastern Mediterranean (Nile River Delta region) over the last 27,000 years. *Paleoceanography*, *25*(1), PA1208. https://doi.org/10.1029/2009PA001740

Ceccopieri, M., Carreira, R. S., Wagener, A. L. R., Hefter, J. H., & Mollenhauer, G. (2018). On the application of alkenone- and GDGT-based temperature proxies in the south-eastern Brazilian continental margin. *Organic Geochemistry*, *126*, 43–56. https://doi.org/10.1016/j.orggeochem.2018.10.009

Chazen, C. R. (2011). *Holocene climate evolution of the eastern tropical Pacific told from high resolution climate records from the Peru margin and equatorial upwelling regions* (Doctoral dissertation). Brown University. https://doi.org/10.7301/Z0D50K7P

Chen, J., Hu, P., Li, X., Yang, Y., Song, J., Li, X., et al. (2018). Impact of water depth on the distribution of iGDGTs in the surface sediments from the northern South China Sea: Applicability of TEX_{86} in marginal seas. *Frontiers of Earth Science*, *12*(1), 95–107. https://doi.org/10.1007/s11707-016-0620-1

Chen, W., Mohtadi, M., Schefuß, E., & Mollenhauer, G. (2014). Organic-geochemical proxies of sea surface temperature in surface sediments of the tropical eastern Indian Ocean. *Deep Sea Research Part I: Oceanographic Research Papers*, *88*, 17–29. https://doi.org/10.1016/j.dsr.2014.03.005

Clark, P. U., Dyke, A. S., Shakun, J. D., Carlson, A. E., Clark, J., Wohlfarth, B., et al. (2009). The Last Glacial Maximum. *Science*, *325*(5941), 710–714. https://doi.org/10.1126/science.1172873

De Rosa, M., Esposito, E., Gambacorta, A., Nicolaus, B., & Bu'Lock, J. D. (1980). Effects of temperature on ether lipid composition of *Caldariella acidophila*. *Phytochemistry*, *19*(5), 827–831. https://doi.org/10.1016/0031-9422(80)85120-X

Elling, F. J., Könneke, M., Lipp, J. S., Becker, K. W., Gagen, E. J., & Hinrichs, K.-U. (2014). Effects of growth phase on the membrane lipid composition of the thaumarchaeon *Nitrosopumilus maritimus* and their implications for archaeal lipid distributions in the marine environment. *Geochimica et Cosmochimica Acta*, *141*, 579–597. https://doi.org/10.1016/j.gca.2014.07.005

Elling, F. J., Könneke, M., Mußmann, M., Greve, A., & Hinrichs, K.-U. (2015). Influence of temperature, pH, and salinity on membrane lipid composition and TEX_{86} of marine planktonic thaumarchaeal isolates. *Geochimica et Cosmochimica Acta*, *171*, 238–255. https://doi.org/10.1016/j.gca.2015.09.004

Erbacher, J., Huber, B. T., Norris, R. D., & Markey, M. (2001). Increased thermohaline stratification as a possible cause for an ocean anoxic event in the Cretaceous period. *Nature*, *409*(6818), 325–327. https://doi.org/10.1038/35053041

Evans, T. W., Könneke, M., Lipp, J. S., Adhikari, R. R., Taubner, H., Elvert, M., & Hinrichs, K.-U. (2018). Lipid biosynthesis of Nitrosopumilus maritimus dissected by lipid specific radioisotope probing (lipid-RIP) under contrasting ammonium supply. *Geochimica et Cosmochimica Acta*, *242*, 51–63. https://doi.org/10.1016/j.gca.2018.09.001

Fallet, U., Castañeda, I. S., Henry-Edwards, A., Richter, T. O., Boer, W., Schouten, S., & Brummer, G.-J. (2012). Sedimentation and burial of organic and inorganic temperature proxies in the Mozambique Channel, SW Indian Ocean. *Deep Sea Research Part I: Oceanographic Research Papers*, *59*, 37–53. https://doi.org/10.1016/j.dsr.2011.10.002

Fietz, S., Ho, S. L., Huguet, C., Rosell-Melé, A., & Martínez-García, A. (2016). Appraising GDGT-based seawater temperature indices in the Southern Ocean. *Organic Geochemistry*, *102*, 93–105. https://doi.org/10.1016/j.orggeochem.2016.10.003

Forster, A., Schouten, S., Baas, M., & Sinninghe Damsté, J. S. (2007). Mid-Cretaceous (Albian–Santonian) sea surface temperature record of the tropical Atlantic Ocean. *Geology*, *35*(10), 919–922. https://doi.org/10.1130/G23874A.1

Forster, A., Schouten, S., Moriya, K., Wilson, P. A., & Sinninghe Damsté, J. S. (2007). Tropical warming and intermittent cooling during the Cenomanian/Turonian oceanic anoxic event 2: Sea surface temperature records from the equatorial Atlantic. *Paleoceanography*, *22*(1), PA1219. https://doi.org/10.1029/2006PA001349

Francis, C. A., Roberts, K. J., Beman, J. M., Santoro, A. E., & Oakley, B. B. (2005). Ubiquity and diversity of ammonia-oxidizing archaea in water columns and sediments of the ocean. *Proceedings of the National Academy of Sciences*, *102*(41), 14683–14688. https://doi.org/10.1073/pnas.0506625102

Ganachaud, A., Cravatte, S., Melet, A., Schiller, A., Holbrook, N. J., Sloyan, B. M., et al. (2014). The Southwest Pacific Ocean circulation and climate experiment (SPICE). *Journal of Geophysical Research: Oceans*, *119*(11), 7660–7686. https://doi.org/10.1002/2013JC009678

Govin, A., Capron, E., Tzedakis, P. C., Verheyden, S., Ghaleb, B., Hillaire-Marcel, C., et al. (2015). Sequence of events from the onset to the demise of the Last Interglacial: Evaluating strengths and limitations of chronologies used in climatic archives. *Quaternary Science Reviews*, *129*, 1–36. https://doi.org/10.1016/j.quascirev.2015.09.018

Hagemann, J. R., Lembke-Jene, L., Lamy, F., Vorrath, M.-E., Kaiser, J., Müller, J., et al. (2023). Collection of GDGT-derived temperatures of 22 new sites at the Chilean margin, supplemented by various previously published sites [Dataset]. *PANGAEA*. https://doi.org/10.1594/PANGAEA.964270

Harning, D. J., Andrews, J. T., Belt, S. T., Cabedo-Sanz, P., Geirsdottir, A., Dildar, N., et al. (2019). Sea ice control on winter subsurface temperatures of the North Iceland Shelf during the Little Ice Age: A TEX_{86} calibration case study. *Paleoceanography and Paleoclimatology*, *34*(6), 1006–1021. https://doi.org/10.1029/2018PA003523

Harning, D. J., Holman, B., Woelders, L., Jennings, A. E., & Sepúlveda, J. (2023). Biomarker characterization of the North Water Polynya, Baffin Bay: Implications for local sea ice and temperature proxies. *Biogeosciences*, *20*(1), 229–249. https://doi.org/10.5194/bg-20-229-2023

Harris, C. R., Millman, K. J., van der Walt, S. J., Gommers, R., Virtanen, P., Cournapeau, D., et al. (2020). Array programming with NumPy. *Nature*, *585*(7825), 357–362. https://doi.org/10.1038/s41586-020-2649-2

Hayward, B. W., Sabaa, A. T., Kolodziej, A., Crundwell, M. P., Steph, S., Scott, G. H., et al. (2012). Planktic foraminifera-based sea-surface temperature record in the Tasman Sea and history of the Subtropical Front around New Zealand, over the last one million years. *Marine Micropaleontology*, *82–83*, 13–27. https://doi.org/10.1016/j.marmicro.2011.10.003

Henley, S. F., Porter, M., Hobbs, L., Braun, J., Guillaume-Castel, R., Venables, E. J., et al. (2020). Nitrate supply and uptake in the Atlantic Arctic sea ice zone: Seasonal cycle, mechanisms and drivers. *Philosophical Transactions of the Royal Society A: Mathematical, Physical and Engineering Sciences*, *378*(2181), 20190361. https://doi.org/10.1098/rsta.2019.0361

Hernández-Sánchez, M. T., Woodward, E. M. S., Taylor, K. W. R., Henderson, G. M., & Pancost, R. D. (2014). Variations in GDGT distributions through the water column in the South East Atlantic Ocean. *Geochimica et Cosmochimica Acta*, *132*, 337–348. https://doi.org/10.1016/j.gca.2014.02.009

Ho, S. L., & Laepple, T. (2015). Glacial cooling as inferred from marine temperature proxies TEX_{86}^{H} and $U_{37}^{K'}$. *Earth and Planetary Science Letters*, *409*, 15–22. https://doi.org/10.1016/j.epsl.2014.10.033

Ho, S. L., & Laepple, T. (2016). Flat meridional temperature gradient in the early Eocene in the subsurface rather than surface ocean. *Nature Geoscience*, *9*(8), 606–610. https://doi.org/10.1038/ngeo2763

Ho, S. L., Mollenhauer, G., Fietz, S., Martínez-Garcia, A., Lamy, F., Rueda, G., et al. (2014). Appraisal of TEX_{86} and TEX_{86}^{L} thermometries in subpolar and polar regions. *Geochimica et Cosmochimica Acta*, *131*, 213–226. https://doi.org/10.1016/j.gca.2014.01.001

Ho, S. L., Yamamoto, M., Mollenhauer, G., & Minagawa, M. (2011). Core top TEX_{86} values in the south and equatorial Pacific. *Organic Geochemistry*, *42*(1), 94–99. https://doi.org/10.1016/j.orggeochem.2010.10.012

Hollis, C. J., Jones, T. D., Anagnostou, E., Bijl, P. K., Cramwinckel, M. J., Cui, Y., et al. (2019). The DeepMIP contribution to PMIP4: Methodologies for selection, compilation and analysis of latest Paleocene and early Eocene climate proxy data, incorporating version 0.1 of the DeepMIP database. *Geoscientific Model Development*, *12*(7), 3149–3206. https://doi.org/10.5194/gmd-12-3149-2019

Hopmans, E. C., Schouten, S., & Sinninghe Damsté, J. S. (2016). The effect of improved chromatography on GDGT-based palaeoproxies. *Organic Geochemistry*, *93*, 1–6. https://doi.org/10.1016/j.orggeochem.2015.12.006

Hopmans, E. C., Weijers, J. W. H., Schefuß, E., Herfort, L., Sinninghe Damsté, J. S., & Schouten, S. (2004). A novel proxy for terrestrial organic matter in sediments based on branched and isoprenoid tetraether lipids. *Earth and Planetary Science Letters*, *224*(1), 107–116. https://doi.org/10.1016/j.epsl.2004.05.012

Hoyer, S., & Hamman, J. (2017). xarray: N-D labeled arrays and datasets in Python. *Journal of Open Research Software*, *5*(1), 10. https://doi.org/10.5334/jors.148

Hu, J., Meyers, P. A., Chen, G., Peng, P., & Yang, Q. (2012). Archaeal and bacterial glycerol dialkyl glycerol tetraethers in sediments from the Eastern Lau Spreading Center, South Pacific Ocean. *Organic Geochemistry*, *43*, 162–167. https://doi.org/10.1016/j.orggeochem.2011.10.012

Huguet, C., Kim, J.-H., Sinninghe Damsté, J. S., & Schouten, S. (2006). Reconstruction of sea surface temperature variations in the Arabian Sea over the last 23 kyr using organic proxies (TEX_{86} and $U_{37}^{K'}$). *Paleoceanography*, *21*(3). https://doi.org/10.1029/2005pa001215

Hunter, J. D. (2007). Matplotlib: A 2D graphics environment. *Computing in Science & Engineering*, *9*(3), 90–95. https://doi.org/10.1109/mcse.2007.55

Hurley, S. J., Elling, F. J., Könneke, M., Buchwald, C., Wankel, S. D., Santoro, A. E., et al. (2016). Influence of ammonia oxidation rate on thaumarchaeal lipid composition and the TEX_{86} temperature proxy. *Proceedings of the National Academy of Sciences*, *113*(28), 7762–7767. https://doi.org/10.1073/pnas.1518534113

Hurley, S. J., Lipp, J. S., Close, H. G., Hinrichs, K.-U., & Pearson, A. (2018). Distribution and export of isoprenoid tetraether lipids in suspended particulate matter from the water column of the Western Atlantic Ocean. *Organic Geochemistry*, *116*, 90–102. https://doi.org/10.1016/j.orggeochem.2017.11.010

Inglis, G. N., Farnsworth, A., Lunt, D., Foster, G. L., Hollis, C. J., Pagani, M., et al. (2015). Descent toward the Icehouse: Eocene sea surface cooling inferred from GDGT distributions. *Paleoceanography*, *30*(7), 1000–1020. https://doi.org/10.1002/2014pa002723

Ivanochko, T. S., Ganeshram, R. S., Brummer, G.-J. A., Ganssen, G., Jung, S. J. A., Moreton, S. G., & Kroon, D. (2005). Variations in tropical convection as an amplifier of global climate change at the millennial scale. *Earth and Planetary Science Letters*, *235*(1), 302–314. https://doi.org/10.1016/j.epsl.2005.04.002

Jaeschke, A., Wengler, M., Hefter, J., Ronge, T. A., Geibert, W., Mollenhauer, G., et al. (2017). A biomarker perspective on dust, productivity, and sea surface temperature in the Pacific sector of the Southern Ocean. *Geochimica et Cosmochimica Acta*, *204*, 120–139. https://doi.org/10.1016/j.gca.2017.01.045

Jia, G., Zhang, J., Chen, J., Peng, P., & Zhang, C. L. (2012). Archaeal tetraether lipids record subsurface water temperature in the South China Sea. *Organic Geochemistry*, *50*, 68–77. https://doi.org/10.1016/j.orggeochem.2012.07.002

Judd, E. J., Tierney, J. E., Huber, B. T., Wing, S. L., Lunt, D. J., Ford, H. L., et al. (2022). The PhanSST global database of Phanerozoic sea surface temperature proxy data. *Scientific Data*, *9*(1), 753. https://doi.org/10.1038/s41597-022-01826-0

Judd, E. J., Tierney, J. E., Lunt, D. J., Montañez, I. P., Huber, B. T., Wing, S. L., & Valdes, P. J. (2024). A 485-million-year history of Earth's surface temperature. *Science*, *385*(6715), eadk3705. https://doi.org/10.1126/science.adk3705

Junium, C. K., Meyers, S. R., & Arthur, M. A. (2018). Nitrogen cycle dynamics in the Late Cretaceous Greenhouse. *Earth and Planetary Science Letters*, *481*, 404–411. https://doi.org/10.1016/j.epsl.2017.10.006

Kaiser, J., Ruggieri, N., Hefter, J., Siegel, H., Mollenhauer, G., Arz, H. W., & Lamy, F. (2014). Lipid biomarkers in surface sediments from the Gulf of Genoa, Ligurian sea (NW Mediterranean sea) and their potential for the reconstruction of palaeo-environments. *Deep Sea Research Part I: Oceanographic Research Papers*, *89*, 68–83. https://doi.org/10.1016/j.dsr.2014.04.009

Kaiser, J., Schouten, S., Kilian, R., Arz, H. W., Lamy, F., & Sinninghe Damsté, J. S. (2015). Isoprenoid and branched GDGT-based proxies for surface sediments from marine, fjord and lake environments in Chile. *Organic Geochemistry*, *89–90*, 117–127. https://doi.org/10.1016/j.orggeochem.2015.10.007

Karner, M. B., DeLong, E. F., & Karl, D. M. (2001). Archaeal dominance in the mesopelagic zone of the Pacific Ocean. *Nature*, *409*(6819), 507–510. https://doi.org/10.1038/35054051

Kawagata, S. (2001). Tasman Front shifts and associated paleoceanographic changes during the last 250,000 years: Foraminiferal evidence from the Lord Howe Rise. *Marine Micropaleontology*, *41*(3), 167–191. https://doi.org/10.1016/S0377-8398(00)00058-X

Kennett, J. P., & Borch, C. (1986). Initial reports of the deep sea drilling project (Vol. *90*). Retrieved from https://api.semanticscholar.org/CorpusID:132141153

Kim, B., & Zhang, Y. G. (2023). Methane index: Towards a quantitative archaeal lipid biomarker proxy for reconstructing marine sedimentary methane fluxes. *Geochimica et Cosmochimica Acta*, *354*, 74–87. https://doi.org/10.1016/j.gca.2023.06.008

Kim, J.-H., Villanueva, L., Zell, C., & Sinninghe Damsté, J. S. (2016). Biological source and provenance of deep-water derived isoprenoid tetraether lipids along the Portuguese continental margin. *Geochimica et Cosmochimica Acta*, *172*, 177–204. https://doi.org/10.1016/j.gca.2015.09.010

Kim, J.-H., Romero, O. E., Lohmann, G., Donner, B., Laepple, T., Haam, E., & Sinninghe Damsté, J. S. (2012). Pronounced subsurface cooling of North Atlantic waters off Northwest Africa during Dansgaard–Oeschger interstadials. *Earth and Planetary Science Letters*, *339–340*, 95–102. https://doi.org/10.1016/j.epsl.2012.05.018

Kim, J.-H., Schouten, S., Hopmans, E. C., Donner, B., & Sinninghe Damsté, J. S. (2008). Global sediment core-top calibration of the TEX_{86} paleothermometer in the ocean. *Geochimica et Cosmochimica Acta*, *72*(4), 1154–1173. https://doi.org/10.1016/j.gca.2007.12.010

Kim, J.-H., Schouten, S., Rodrigo-Gámiz, M., Rampen, S., Marino, G., Huguet, C., et al. (2015). Influence of deep-water derived isoprenoid tetraether lipids on the TEX_{86}^{H} paleothermometer in the Mediterranean Sea. *Geochimica et Cosmochimica Acta*, *150*, 125–141. https://doi.org/10.1016/j.gca.2014.11.017

Kim, J.-H., van der Meer, J., Schouten, S., Helmke, P., Willmott, V., Sangiorgi, F., et al. (2010). New indices and calibrations derived from the distribution of crenarchaeal isoprenoid tetraether lipids: Implications for past sea surface temperature reconstructions. *Geochimica et Cosmochimica Acta*, *74*(16), 4639–4654. https://doi.org/10.1016/j.gca.2010.05.027

Kusch, S., Rethemeyer, J., Hopmans, E. C., Wacker, L., & Mollenhauer, G. (2016). Factors influencing 14C concentrations of algal and archaeal lipids and their associated sea surface temperature proxies in the Black Sea. *Geochimica et Cosmochimica Acta*, *188*, 35–57. https://doi.org/10.1016/j.gca.2016.05.025

Kuypers, M. M. M., Blokker, P., Erbacher, J., Kinkel, H., Pancost, R. D., Schouten, S., & Sinninghe Damsté, J. S. (2001). Massive expansion of marine archaea during a mid-Cretaceous oceanic anoxic event. *Science*, *293*(5527), 92–95. https://doi.org/10.1126/science.1058424

Lamping, N., Müller, J., Hefter, J., Mollenhauer, G., Haas, C., Shi, X., et al. (2021). Evaluation of lipid biomarkers as proxies for sea ice and ocean temperatures along the Antarctic continental margin. *Climate of the Past*, *17*(5), 2305–2326. https://doi.org/10.5194/cp-17-2305-2021

Leider, A., Hinrichs, K.-U., Mollenhauer, G., & Versteegh, G. J. M. (2010). Core-top calibration of the lipid-based $U_{37}^{K'}$ and TEX_{86} temperature proxies on the southern Italian shelf (SW Adriatic Sea, Gulf of Taranto). *Earth and Planetary Science Letters*, *300*(1), 112–124. https://doi.org/10.1016/j.epsl.2010.09.042

Lengger, S. K., Hopmans, E. C., Sinninghe Damsté, J. S., & Schouten, S. (2014). Fossilization and degradation of archaeal intact polar tetraether lipids in deeply buried marine sediments (Peru Margin). *Geobiology*, *12*(3), 212–220. https://doi.org/10.1111/gbi.12081

Lisiecki, L. E., & Raymo, M. E. (2005). A Pliocene-Pleistocene stack of 57 globally distributed benthic $\delta^{18}O$ records. *Paleoceanography*, *20*(1), PA1003. https://doi.org/10.1029/2004pa001071

Liu, X.-L., Zhu, C., Wakeham, S. G., & Hinrichs, K.-U. (2014). In situ production of branched glycerol dialkyl glycerol tetraethers in anoxic marine water columns. *Marine Chemistry*, *166*, 1–8. https://doi.org/10.1016/j.marchem.2014.08.008

Lo, L., Belt, S. T., Lattaud, J., Friedrich, T., Zeeden, C., Schouten, S., et al. (2018). Precession and atmospheric CO_2 modulated variability of sea ice in the central Okhotsk Sea since 130,000 years ago. *Earth and Planetary Science Letters*, *488*, 36–45. https://doi.org/10.1016/j.epsl.2018.02.005

Locarnini, R. A., Mishonov, A. V., Baranova, O. K., Reagan, J. R., Boyer, T. P., Seidov, D., et al. (2024). World ocean atlas 2023, volume 1: Temperature.

Lü, X., Yang, H., Song, J., Versteegh, G. J. M., Li, X., Yuan, H., et al. (2014). Sources and distribution of isoprenoid glycerol dialkyl glycerol tetraethers (GDGTs) in sediments from the east coastal sea of China: Application of GDGT-based paleothermometry to a shallow marginal sea. *Organic Geochemistry*, *75*, 24–35. https://doi.org/10.1016/j.orggeochem.2014.06.007

Martens-Habbena, W., Berube, P. M., Urakawa, H., de la Torre, J. R., & Stahl, D. A. (2009). Ammonia oxidation kinetics determine niche separation of nitrifying Archaea and Bacteria. *Nature*, *461*(7266), 976–979. https://doi.org/10.1038/nature08465

Martínez, J. (1994). Late Pleistocene palaeocenography of the Tasman Sea: Implications for the dynamics of the warm pool in the western Pacific. *Palaeogeography, Palaeoclimatology, Palaeoecology*, *112*(1), 19–62. https://doi.org/10.1016/0031-0182(94)90133-3

Martínez, J. (1997). Decreasing influence of subantarctic mode water north of the tasman front over the past 150 kyr. *Palaeogeography, Palaeoclimatology, Palaeoecology*, *131*(3–4), 355–364. https://doi.org/10.1016/S0031-0182(97)00011-4

McKinney, W. (2010). Data structures for statistical computing in Python. In *Proceedings of the 9th Python in science conference* (Vol. 445, pp. 56–61). https://doi.org/10.25080/majora-92bf1922-00a

McManus, J. F., Francois, R., Gherardi, J.-M., Keigwin, L. D., & Brown-Leger, S. (2004). Collapse and rapid resumption of Atlantic meridional circulation linked to deglacial climate changes. *Nature*, *428*(6985), 834–837. https://doi.org/10.1038/nature02494

Nelson, C., Hendy, C., & Cuthbertson, A. (1994). Oxygen isotope evidence for climatic contrasts between tasman sea and southwest Pacific ocean during the late quaternary. In *Tasman Sea Conference* (pp. 181–196).

Nelson, C. S., Hendy, C. H., & Cuthbertson, A. M. (1993). *Compendium of stable oxygen and carbon isotope data for the late quaternary interval of deep-sea cores from the New Zealand sector of the Tasman Sea and Southwest Pacific Ocean*. Department of Earth Sciences, University of Waikato.

Nieto-Moreno, V., Martínez-Ruiz, F., Willmott, V., García-Orellana, J., Masqué, P., & Sinninghe Damsté, J. S. (2013). Climate conditions in the westernmost Mediterranean over the last two millennia: An integrated biomarker approach. *Organic Geochemistry*, *55*, 1–10. https://doi.org/10.1016/j.orggeochem.2012.11.001

Pan, A., Yang, Q., Zhou, H., Ji, F., Wang, H., & Pancost, R. D. (2016). A diagnostic GDGT signature for the impact of hydrothermal activity on surface deposits at the Southwest Indian Ridge. *Organic Geochemistry*, *99*, 90–101. https://doi.org/10.1016/j.orggeochem.2016.07.001

Park, Y.-H., Yamamoto, M., Nam, S.-I., Irino, T., Polyak, L., Harada, N., et al. (2014). Distribution, source and transportation of glycerol dialkyl glycerol tetraethers in surface sediments from the western Arctic Ocean and the northern Bering Sea. *Marine Chemistry*, *165*, 10–24. https://doi.org/10.1016/j.marchem.2014.07.001

Paulot, F., Jacob, D. J., Johnson, M. T., Bell, T. G., Baker, A. R., Keene, W. C., et al. (2015). Global oceanic emission of ammonia: Constraints from seawater and atmospheric observations. *Global Biogeochemical Cycles*, *29*(8), 1165–1178. https://doi.org/10.1002/2015GB005106

Pedregosa, F., Varoquaux, G., Gramfort, A., Michel, V., Thirion, B., Grisel, O., et al. (2011). Scikit-learn: Machine learning in python. *Journal of Machine Learning Research*, *12*, 2825–2830.

Peng, X., Fuchsman, C. A., Jayakumar, A., Warner, M. J., Devol, A. H., & Ward, B. B. (2016). Revisiting nitrification in the Eastern Tropical South Pacific: A focus on controls. *Journal of Geophysical Research: Oceans*, *121*(3), 1667–1684. https://doi.org/10.1002/2015JC011455

Perruche, C. (2018). *Product user manual for the global ocean biogeochemistry hindcast global_reanalysis_bio_001_029. version 1*. Copernicus Marine Environment Monitoring Service. https://doi.org/10.25607/OBP-490

Polik, C. A., Elling, F. J., & Pearson, A. (2018). Impacts of paleoecology on the TEX_{86} sea surface temperature proxy in the Pliocene-Pleistocene Mediterranean Sea. *Paleoceanography and Paleoclimatology*, *33*(12), 1472–1489. https://doi.org/10.1029/2018pa003494

Polovina, J. J., Dunne, J. P., Woodworth, P. A., & Howell, E. A. (2011). Projected expansion of the subtropical biome and contraction of the temperate and equatorial upwelling biomes in the North Pacific under global warming. *ICES Journal of Marine Science*, *68*(6), 986–995. https://doi.org/10.1093/icesjms/fsq198

Prahl, F. G., & Wakeham, S. G. (1987). Calibration of unsaturation patterns in long-chain ketone compositions for palaeotemperature assessment. *Nature*, *330*(6146), 367–369. https://doi.org/10.1038/330367a0

Proctor, C., Coupel, P., Casciotti, K., Tremblay, J.-E., Zakem, E., Arrigo, K. R., & Mills, M. M. (2023). Light, ammonium, pH, and phytoplankton competition as environmental factors controlling nitrification. *Limnology and Oceanography*, *68*(7), 1490–1503. https://doi.org/10.1002/lno.12359

Python 3.10. (2010). *Python 3.10*. Python Software Foundation. Retrieved from https://www.python.org/

Qin, W., Carlson, L. T., Armbrust, E. V., Devol, A. H., Moffett, J. W., Stahl, D. A., & Ingalls, A. E. (2015). Confounding effects of oxygen and temperature on the TEX_{86} signature of marine Thaumarchaeota. *Proceedings of the National Academy of Sciences*, *112*(35), 10979–10984. https://doi.org/10.1073/pnas.1501568112

Rasmussen, S. O., Andersen, K. K., Svensson, A. M., Steffensen, J. P., Vinther, B. M., Clausen, H. B., et al. (2006). A new Greenland ice core chronology for the last glacial termination. *Journal of Geophysical Research*, *111*(D6). https://doi.org/10.1029/2005JD006079

Rattanasriampaipong, R., Tierney, J., & Abell, J. (2025). Supplementary Data for 'A nutrient effect on the TEX_{86} paleotemperature proxy' [Dataset]. *Zenodo*. https://doi.org/10.5281/zenodo.14806962

Rattanasriampaipong, R., Zhang, Y. G., Pearson, A., Hedlund, B., & Zhang, S. (2022a). Expanded compilations of isoprenoidal glycerol dialkyl glycerol tetraethers (GDGTs) in supplement to Rattanasriampaipong et al. "Archaeal lipids trace ecology and evolution of marine ammonia-oxidizing archaea" [Dataset]. *figshare*. https://doi.org/10.6084/m9.figshare.20272866.v3

Rattanasriampaipong, R., Zhang, Y. G., Pearson, A., Hedlund, B. P., & Zhang, S. (2022b). Archaeal lipids trace ecology and evolution of marine ammonia-oxidizing archaea. *Proceedings of the National Academy of Sciences*, *119*(31), e2123193119. https://doi.org/10.1073/pnas.2123193119

Richey, J. N., Hollander, D. J., Flower, B. P., & Eglinton, T. I. (2011). Merging late Holocene molecular organic and foraminiferal-based geochemical records of sea surface temperature in the Gulf of Mexico. *Paleoceanography*, *26*(1). https://doi.org/10.1029/2010PA002000

Richey, J. N., & Tierney, J. E. (2016). GDGT and alkenone flux in the northern Gulf of Mexico: Implications for the TEX_{86} and $U_{37}^{K'}$ paleothermometers. *Paleoceanography*, *31*(12), 1547–1561. https://doi.org/10.1002/2016pa003032

Rodrigo-Gámiz, M., Rampen, S. W., de Haas, H., Baas, M., Schouten, S., & Sinninghe Damsté, J. S. (2015). Constraints on the applicability of the organic temperature proxies $U_{37}^{K'}$, TEX_{86} and LDI in the subpolar region around Iceland. *Biogeosciences*, *12*(22), 6573–6590. https://doi.org/10.5194/bg-12-6573-2015

Sarmiento, J. L., & Gruber, N. (2006). Ocean biogeochemical dynamics. In *Ocean biogeochemical dynamics* (p. 528). Princeton University Press.

Schouten, S., Forster, A., Panoto, F. E., & Sinninghe Damsté, J. S. (2007). Towards calibration of the TEX_{86} palaeothermometer for tropical sea surface temperatures in ancient greenhouse worlds. *Organic Geochemistry*, *38*(9), 1537–1546. https://doi.org/10.1016/j.orggeochem.2007.05.014

Schouten, S., Hopmans, E. C., Schefuss, E., & Sinninghe Damsté, J. S. (2002). Distributional variations in marine crenarchaeotal membrane lipids: A new tool for reconstructing ancient sea water temperatures? *Earth and Planetary Science Letters*, *204*(1–2), 265–274. https://doi.org/10.1016/s0012-821x(02)00979-2

Schukies, J. (2018). Concentrations of glycerol dialkyl glycerol tetraethers (GDGTs) in core top sediments from continental slope off Newfoundland, Orphan Knoll Region [Dataset]. *PANGAEA*. https://doi.org/10.1594/PANGAEA.894305

Schulte, S., & Müller, P. J. (2001). Variations of sea surface temperature and primary productivity during Heinrich and Dansgaard-Oeschger events in the northeastern Arabian Sea. *Geo-Marine Letters*, *21*(3), 168–175. https://doi.org/10.1007/s003670100080

Seierstad, I. K., Abbott, P. M., Bigler, M., Blunier, T., Bourne, A. J., Brook, E., et al. (2014). Consistently dated records from the Greenland GRIP, GISP2 and NGRIP ice cores for the past 104 ka reveal regional millennial-scale $\delta^{18}O$ gradients with possible Heinrich event imprint. *Quaternary Science Reviews*, *106*, 29–46. https://doi.org/10.1016/j.quascirev.2014.10.032

Seki, O., Bendle, J. A., Harada, N., Kobayashi, M., Sawada, K., Moossen, H., et al. (2014). Assessment and calibration of TEX_{86} paleothermometry in the Sea of Okhotsk and sub-polar North Pacific region: Implications for paleoceanography. *Progress in Oceanography*, *126*, 254–266. https://doi.org/10.1016/j.pocean.2014.04.013

Seki, O., Sakamoto, T., Sakai, S., Schouten, S., Hopmans, E. C., Sinninghe Damste, J. S., & Pancost, R. D. (2009). Large changes in seasonal sea ice distribution and productivity in the Sea of Okhotsk during the deglaciations. *Geochemistry, Geophysics, Geosystems*, *10*(10),Q10007. https://doi.org/10.1029/2009GC002613

Shevenell, A. E., Ingalls, A. E., Domack, E. W., & Kelly, C. (2011). Holocene Southern Ocean surface temperature variability west of the Antarctic Peninsula. *Nature*, *470*(7333), 250–254. https://doi.org/10.1038/nature09751

Siegel, D. A., DeVries, T., Cetinić, I., & Bisson, K. M. (2023). Quantifying the ocean's biological pump and its carbon cycle impacts on global scales. *Annual Review of Marine Science*, *15*(1), 329–356. https://doi.org/10.1146/annurev-marine-040722-115226

Sikes, E. L., Howard, W. R., Samson, C. R., Mahan, T. S., Robertson, L. G., & Volkman, J. K. (2009). Southern Ocean seasonal temperature and Subtropical Front movement on the South Tasman Rise in the late Quaternary. *Paleoceanography*, *24*(2), PA2201. https://doi.org/10.1029/2008PA001659

Sinninghe Damsté, J. S. (2016). Spatial heterogeneity of sources of branched tetraethers in shelf systems: The geochemistry of tetraethers in the Berau River delta (Kalimantan, Indonesia). *Geochimica et Cosmochimica Acta*, *186*, 13–31. https://doi.org/10.1016/j.gca.2016.04.033

Sinninghe Damsté, J. S., Ossebaar, J., Schouten, S., & Verschuren, D. (2012). Distribution of tetraether lipids in the 25-ka sedimentary record of Lake Challa: Extracting reliable TEX_{86} and MBT/CBT palaeotemperatures from an equatorial African lake. *Quaternary Science Reviews*, *50*, 43–54. https://doi.org/10.1016/j.quascirev.2012.07.001

Sinninghe Damsté, J. S., Schouten, S., Hopmans, E. C., van Duin, A. C. T., & Geenevasen, J. A. J. (2002). Crenarchaeol: The characteristic core glycerol dibiphytanyl glycerol tetraether membrane lipid of cosmopolitan pelagic crenarchaeota. *Journal of Lipid Research*, *43*(10), 1641–1651. https://doi.org/10.1194/jlr.m200148-jlr200

Sinninghe Damsté, J. S., van Bentum, E. C., Reichart, G.-J., Pross, J., & Schouten, S. (2010). A CO_2 decrease-driven cooling and increased latitudinal temperature gradient during the mid-Cretaceous Oceanic Anoxic Event 2. *Earth and Planetary Science Letters*, *293*(1), 97–103. https://doi.org/10.1016/j.epsl.2010.02.027

Sinninghe Damsté, J. S., Warden, L. A., Berg, C., Jürgens, K., & Moros, M. (2022). Evaluation of the distributions of hydroxylated glycerol dibiphytanyl glycerol tetraethers (GDGTs) in Holocene Baltic Sea sediments for reconstruction of sea surface temperature: The effect of changing salinity. *Climate of the Past*, *18*(10), 2271–2288. https://doi.org/10.5194/cp-18-2271-2022

Sintes, E., Bergauer, K., De Corte, D., Yokokawa, T., & Herndl, G. J. (2013). Archaeal amoA gene diversity points to distinct biogeography of ammonia-oxidizing Crenarchaeota in the ocean. *Environmental Microbiology*, *15*(5), 1647–1658. https://doi.org/10.1111/j.1462-2920.2012.02801.x

Sloyan, B. M., & O'Kane, T. J. (2015). Drivers of decadal variability in the Tasman Sea. *Journal of Geophysical Research: Oceans*, *120*(5), 3193–3210. https://doi.org/10.1002/2014JC010550

Smith, J. M., Casciotti, K. L., Chavez, F. P., & Francis, C. A. (2014). Differential contributions of archaeal ammonia oxidizer ecotypes to nitrification in coastal surface waters. *The ISME Journal*, *8*(8), 1704–1714. https://doi.org/10.1038/ismej.2014.11

Smith, M., De Deckker, P., Rogers, J., Brocks, J., Hope, J., Schmidt, S., et al. (2013). Comparison of $U_{37}^{K'}$, TEX_{86}^{H} and LDI temperature proxies for reconstruction of south-east Australian ocean temperatures. *Organic Geochemistry*, *64*, 94–104. https://doi.org/10.1016/j.orggeochem.2013.08.015

Sonzogni, C., Bard, E., & Rostek, F. (1998). Tropical sea-surface temperatures during the last glacial period: A view based on alkenones in Indian Ocean sediments. *Quaternary Science Reviews*, *17*(12), 1185–1201. https://doi.org/10.1016/S0277-3791(97)00099-1

Sutherland, R., Dickens, G. R., Blum, P., & the Expedition 317 Scientists. (2019). Tasman Frontier Subduction Initiation and Paleogene Climate. *Proceedings of the International Ocean Discovery Program*, *371*, 1–44.

Suthhof, A., Ittekkot, V., & Gaye-Haake, B. (2001). Millennial-scale oscillation of denitrification intensity in the Arabian Sea during the Late Quaternary and its potential influence on atmospheric N_2O and global climate. *Global Biogeochemical Cycles*, *15*(3), 637–649. https://doi.org/10.1029/2000GB001337

Talley, L. D., Pickard, G. L., Emery, W. J., & Swift, J. H. (2011). *Descriptive physical oceanography: An introduction* (6th ed.). Academic Press. https://doi.org/10.1016/C2009-0-24322-4

Tang, W., Ward, B. B., Beman, M., Bristow, L., Clark, D., Fawcett, S., et al. (2023). Database of nitrification and nitrifiers in the global ocean. *Earth System Science Data*, *15*(11), 5039–5077. https://doi.org/10.5194/essd-15-5039-2023

Taylor, K. W. R., Huber, M., Hollis, C. J., Hernandez-Sanchez, M. T., & Pancost, R. D. (2013). Re-evaluating modern and Palaeogene GDGT distributions: Implications for SST reconstructions. *Global and Planetary Change*, *108*, 158–174. https://doi.org/10.1016/j.gloplacha.2013.06.011

Tesdal, J.-E., Galbraith, E. D., & Kienast, M. (2013). Nitrogen isotopes in bulk marine sediment: Linking seafloor observations with subseafloor records. *Biogeosciences*, *10*(1), 101–118. https://doi.org/10.5194/bg-10-101-2013

Tierney, J. E., Pausata, F. S. R., & DeMenocal, P. (2016). Deglacial Indian monsoon failure and North Atlantic stadials linked by Indian Ocean surface cooling. *Nature Geoscience*, *9*(1), 46–50. https://doi.org/10.1038/ngeo2603

Tierney, J. E., Poulsen, C. J., Montañez, I. P., Bhattacharya, T., Feng, R., Ford, H. L., et al. (2020). Past climates inform our future. *Science*, *370*(6517), eaay3701. https://doi.org/10.1126/science.aay3701

Tierney, J. E., & Tingley, M. P. (2014). A Bayesian, spatially-varying calibration model for the TEX_{86} proxy. *Geochimica et Cosmochimica Acta*, *127*, 83–106. https://doi.org/10.1016/j.gca.2013.11.026

Tierney, J. E., & Tingley, M. P. (2015a). NOAA/WDS Paleoclimatology - Global TEX_{86} Surface Sediment Database [Dataset]. *NOAA National Centers for Environmental Information*. https://doi.org/10.25921/wt2r-sc81

Tierney, J. E., & Tingley, M. P. (2015b). A TEX 86 surface sediment database and extended Bayesian calibration. *Scientific Data*, *2*(1), 1–10. https://doi.org/10.1038/sdata.2015.29

Tierney, J. E., & Tingley, M. P. (2018). BAYSPLINE: A New calibration for the alkenone paleothermometer. *Paleoceanography and Paleoclimatology*, *33*(3), 281–301. https://doi.org/10.1002/2017PA003201

Tierney, J. E., Ummenhofer, C. C., & DeMenocal, P. B. (2015). Past and future rainfall in the Horn of Africa. *Science Advances*, *1*(9), e1500682. https://doi.org/10.1126/sciadv.1500682

Tilburg, C. E., Hurlburt, H. E., O'Brien, J. J., & Shriver, J. F. (2001). The dynamics of the East Australian current system: The Tasman front, the east Auckland current, and the East Cape current. *Journal of Physical Oceanography*, *31*, 2917–2943. https://doi.org/10.1175/1520-0485(2001)031⟨2917:TDOTEA⟩2.0.CO;2

Tilburg, C. E., Subrahmanyam, B., & O'Brien, J. J. (2002). Ocean color variability in the Tasman Sea. *Geophysical Research Letters*, *29*(10), 124–125. https://doi.org/10.1029/2001GL014071

Trommer, G., Siccha, M., van der Meer, M. T. J., Schouten, S., Sinninghe Damsté, J. S., Schulz, H., et al. (2009). Distribution of Crenarchaeota tetraether membrane lipids in surface sediments from the Red Sea. *Organic Geochemistry*, *40*(6), 724–731. https://doi.org/10.1016/j.orggeochem.2009.03.001

Tyrrell, T. (1999). The relative influences of nitrogen and phosphorus on oceanic primary production. *Nature*, *400*(6744), 525–531. https://doi.org/10.1038/22941

Uda, I., Sugai, A., Itoh, Y. H., & Itoh, T. (2001). Variation in molecular species of polar lipids from *Thermoplasma acidophilum* depends on growth temperature. *Lipids*, *36*(1), 103–105. https://doi.org/10.1007/s11745-001-0914-2

van der Weijst, C. M. H., van der Laan, K. J., Peterse, F., Reichart, G.-J., Sangiorgi, F., Schouten, S., et al. (2022). A 15-million-year surface- and subsurface-integrated TEX_{86} temperature record from the eastern equatorial Atlantic. *Climate of the Past*, *18*(8), 1947–1962. https://doi.org/10.5194/cp-18-1947-2022

van Helmond, N. A. G. M., Sluijs, A., Reichart, G.-J., Sinninghe Damsté, J. S., Slomp, C. P., & Brinkhuis, H. (2014). A perturbed hydrological cycle during Oceanic Anoxic Event 2. *Geology*, *42*(2), 123–126. https://doi.org/10.1130/G34929.1

Varma, D., Hopmans, E. C., van Kemenade, Z. R., Kusch, S., Berg, S., Bale, N. J., et al. (2024). Evaluating isoprenoidal hydroxylated GDGT-based temperature proxies in surface sediments from the global ocean. *Geochimica et Cosmochimica Acta*, *370*, 113–127. https://doi.org/10.1016/j.gca.2023.12.019

Varma, D., Hopmans, E. C., van Kemenda, Z. R., Kusch, S., Berg, S., Bale, N. J., et al. (2024). OHGDGT global surface sediment data [Dataset]. *PANGAEA*. https://doi.org/10.1594/PANGAEA.964885

Verleye, T. J. (2011). *The late Quaternary palaeoenvironmental changes along the western South-American continental slope: A reconstruction based on dinoflagellate cysts and* TEX_{86} (PhD Thesis). Ghent University. Retrieved from https://www.vliz.be/en/imis?module=ref&refid=210274

Villanueva, L., Schouten, S., & Sinninghe Damsté, J. S. (2015). Depth-related distribution of a key gene of the tetraether lipid biosynthetic pathway in marine Thaumarchaeota. *Environmental Microbiology*, *17*(10), 3527–3539. https://doi.org/10.1111/1462-2920.12508

Virtanen, P., Gommers, R., Oliphant, T. E., Haberland, M., Reddy, T., Cournapeau, D., et al. (2020). Scipy 1.0: Fundamental algorithms for scientific computing in python. *Nature Methods*, *17*(3), 261–272. https://doi.org/10.1038/s41592-019-0686-2

Ward, B. B. (2008). In D. G. Capone, D. A. Bronk, M. R. Mulholland, & E. J. Carpenter (Eds.), *Chapter 5 - Nitrification in Marine Systems* (pp. 199–261). Academic Press. https://doi.org/10.1016/B978-0-12-372522-6.00005-0

Ward, B. B. (2011). Nitrification in the Ocean. In *Nitrification* (pp. 323–345). https://doi.org/10.1128/9781555817145.ch13

Wei, B., Jia, G., Hefter, J., Kang, M., Park, E., Wang, S., & Mollenhauer, G. (2020). Comparison of the $U_{37}^{K'}$, LDI, TEX_{86}^{H}, and RI-OH temperature proxies in sediments from the northern shelf of the South China Sea. *Biogeosciences*, *17*(17), 4489–4508. https://doi.org/10.5194/bg-17-4489-2020

Wei, Y., Wang, J., Liu, J., Dong, L., Li, L., Wang, H., et al. (2011). Spatial variations in archaeal lipids of surface water and core-top sediments in the South China Sea and their implications for paleoclimate studies. *Applied and Environmental Microbiology*, *77*(21), 7479–7489. https://doi.org/10.1128/aem.00580-11

Weijers, J. W. H., Schouten, S., Spaargaren, O. C., & Sinninghe Damsté, J. S. (2006). Occurrence and distribution of tetraether membrane lipids in soils: Implications for the use of the TEX_{86} proxy and the BIT index. *Organic Geochemistry*, *37*(12), 1680–1693. https://doi.org/10.1016/j.orggeochem.2006.07.018

Wu, W., Tan, W., Zhou, L., Yang, H., & Xu, Y. (2012). Sea surface temperature variability in southern Okinawa Trough during last 2700 years. *Geophysical Research Letters*, *39*(14), L14705. https://doi.org/10.1029/2012GL052749

Wuchter, C., Abbas, B., Coolen, M. J. L., Herfort, L., van Bleijswijk, J., Timmers, P., et al. (2006). Archaeal nitrification in the ocean. *Proceedings of the National Academy of Sciences*, *103*(33), 12317–12322. https://doi.org/10.1073/pnas.0600756103

Wuchter, C., Schouten, S., Coolen, M. J. L., & Sinninghe Damsté, J. S. (2004). Temperature-dependent variation in the distribution of tetraether membrane lipids of marine Crenarchaeota: Implications for TEX_{86} paleothermometry. *Paleoceanography*, *19*(4), PA4028. https://doi.org/10.1029/2004PA001041

Yang, H., Lohmann, G., Krebs-Kanzow, U., Ionita, M., Shi, X., Sidorenko, D., et al. (2020). Poleward shift of the major ocean gyres detected in a warming climate. *Geophysical Research Letters*, *47*(5), e2019GL085868. https://doi.org/10.1029/2019GL085868

Yang, Y., Gao, C., Dang, X., Ruan, X., Lü, X., Xie, S., et al. (2018). Assessing hydroxylated isoprenoid GDGTs as a paleothermometer for the tropical South China Sea. *Organic Geochemistry*, *115*, 156–165. https://doi.org/10.1016/j.orggeochem.2017.10.014

Yool, A., Martin, A. P., Fernández, C., & Clark, D. R. (2007). The significance of nitrification for oceanic new production. *Nature*, *447*(7147), 999–1002. https://doi.org/10.1038/nature05885

Zachos, J., Dickens, G. R., & Zeebe, R. E. (2008). An early Cenozoic perspective on greenhouse warming and carbon-cycle dynamics. *Nature*, *451*(7176), 279–283. https://doi.org/10.1038/nature06588

Zachos, J., Pagani, M., Sloan, L., Thomas, E., & Billups, K. (2001). Trends, rhythms, and aberrations in global climate 65 Ma to present. *Science*, *292*(5517), 686–693. https://doi.org/10.1126/science.1059412

Zell, C., Kim, J.-H., Hollander, D., Lorenzoni, L., Baker, P., Silva, C. G., et al. (2014). Sources and distributions of branched and isoprenoid tetraether lipids on the Amazon shelf and fan: Implications for the use of GDGT-based proxies in marine sediments. *Geochimica et Cosmochimica Acta*, *139*, 293–312. https://doi.org/10.1016/j.gca.2014.04.038

Zhang, Y. G., & Liu, X. (2018). Export depth of the TEX_{86} signal. *Paleoceanography and Paleoclimatology*, *33*(7), 666–671. https://doi.org/10.1029/2018PA003337

Zhang, Y. G., Zhang, C. L., Liu, X.-L., Li, L., Hinrichs, K.-U., & Noakes, J. E. (2011). Methane index: A tetraether archaeal lipid biomarker indicator for detecting the instability of marine gas hydrates. *Earth and Planetary Science Letters*, *307*(3–4), 525–534. https://doi.org/10.1016/j.epsl.2011.05.031

Zhou, H., Hu, J., Spiro, B., Peng, P., & Tang, J. (2014). Glycerol dialkyl glycerol tetraethers in surficial coastal and open marine sediments around China: Indicators of sea surface temperature and effects of their sources. *Palaeogeography, Palaeoclimatology, Palaeoecology*, *395*, 114–121. https://doi.org/10.1016/j.palaeo.2013.12.006